Xiangchun Xuan

Department of Mechanical Engineering, Clemson University, Clemson, SC, USA

Received January 21, 2019
Revised February 22, 2019
Accepted February 24, 2019

Review

Recent advances in direct current electrokinetic manipulation of particles for microfluidic applications

Microfluidic devices have been extensively used to achieve precise transport and placement of a variety of particles for numerous applications. A range of force fields have thus far been demonstrated to control the motion of particles in microchannels. Among them, electric field-driven particle manipulation may be the most popular and versatile technique because of its general applicability and adaptability as well as the ease of operation and integration into lab-on-a-chip systems. This article is aimed to review the recent advances in direct current (DC) (and as well DC-biased alternating current) electrokinetic manipulation of particles for microfluidic applications. The electric voltages are applied through electrodes that are positioned into the distant channel-end reservoirs for a concurrent transport of the suspending fluid and manipulation of the suspended particles. The focus of this review is upon the cross-stream nonlinear electrokinetic motions of particles in the linear electroosmotic flow of fluids, which enable the diverse control of particle transport in microchannels via the wall-induced electrical lift and/or the insulating structure-induced dielectrophoretic force.

Keywords:
Dielectrophoresis / Electrical lift / Electroosmosis / Electrophoresis / Particle manipulation
DOI 10.1002/elps.201900048

1 Introduction

Since the development of the PDMS-based soft lithography technique two decades ago [1], microfluidic devices have been extensively used to focus [2], trap [3], concentrate [4], and separate [5] particles (varying from nano to micro, biological to synthetic, rigid to soft, etc.) for many biomedical, chemical, and environmental applications [6, 7]. Compared to their macroscopic counterparts, microfluidic devices have the following advantages: (1) precise fluid control because of the small Reynolds number flow; (2) low sample consumption because of the small volume of microchannels; (3) accurate particle manipulation because of the strong confinement effect (as a result of the comparable particle and channel sizes), and as well the small Reynolds number, and so on. [8, 9]. A variety of force fields, ranging from the ubiquitous gravity [10] to centrifugal [11], acoustic [12], electric [13], magnetic [14], optical [15], and flow [16] fields, have thus far been demonstrated to manipulate particles for microfluidic applications. Each of these fields generates a particle motion, whose dependence on particle size and other physicochemical properties is significantly different from each other (Table 1). Among them, the electric control of particle motion in microchannels may be the most popular and versatile technique because of its general applicability and adaptability [17–19]. Moreover, such electrokinetic manipulations of particles are easy to operate, reconfigure, and integrate into lab-on-a-chip systems for numerous other applications such as point-of-care technologies [20–22].

Both alternating current (AC) and direct current (DC) electric fields have been widely used to manipulate particles in microfluidic devices [25–27]. Traditionally, AC electric fields (especially of high frequencies) are applied across in-channel metallic microelectrodes to generate particle dielectrophoresis (DEP) [28, 29], which, as compared to DC electric fields, can significantly suppress electrochemical reactions on electrode surfaces [30, 31]. DC electric fields are involved in capillary (zone) electrophoresis [32], which drive both fluid electroosmosis and particle electrophoresis through straight uniform (both geometrically and physicochemically) microchannels [33, 34]. A hydrodynamic pumping of the particulate solution, which is required in nearly all other field

Correspondence: Professor Xiangchun Xuan, Department of Mechanical Engineering, Clemson University, Clemson, SC 29634-0921, USA
E-mail: xcxuan@clemson.edu

Abbreviations: **3DiDEP**, three-dimensional iDEP; **AC**, alternating current; **C-iDEP**, curvature-induced dielectrophoresis; **CM**, Clausius–Mossotti factor; **DC**, direct current; **DEP**, dielectrophoresis; **eDEP**, electrode-based dielectrophoresis; **EDL**, electric double layer; **iDEP**, insulator-based dielectrophoresis; **LTM**, Lagrangian Tracking Method; **nDEP**, negative DEP; **pDEP**, positive DEP; **rDEP**, reservoir-based dielectrophoresis

Color Online: See the article online to view Figs. 1–20 in color.

Table 1. Comparison of force fields for microfluidic manipulation of particles of radius a

Field	Induced particle motion and its property dependence	Scaling[a)]
Gravity[b)]	Sedimentation and centrifugation: Relative density of particles and fluids [11]	a^2
Acoustic	Acoustophoresis: Relative density and compressibility of particles and fluids [12]	a^2
Electric	*Electrophoresis: Electric charge on particle surface* [23]	*Weak*
	Dielectrophoresis: Relative permittivity and conductivity of particles and fluids [13]	a^2
Magnetic	Magnetophoresis: Relative magnetic permeability of particles and fluids [14]	a^2
Optical	Optophoresis: Relative refractive index of particles and fluids [15]	a^5
Flow	Dean-flow drag-induced particle motion [16]	None[c)]
	Lift-induced cross-stream particle motion [16]	a^3

a) The presented scales are each obtained by balancing the relevant force field with Stokes' drag.
b) Gravitational or centrifugal acceleration.
c) Particles move along with fluids at small Reynolds numbers [24].

control methods, thus becomes unnecessary in DC electric field-mediated applications [35, 36]. If the microchannel is geometrically nonuniform or nonstraight, DC electric fields can also generate a dielectrophoretic particle motion, which is the underlying mechanism of the rapidly growing insulator-based DEP (iDEP) technique [37, 38]. In addition, DC-biased AC electric fields have been increasingly used to control the motion of particles in microchannels. Both the DC and AC voltages are applied through electrodes (e.g., platinum wires) that are positioned into the channel-end reservoirs for concurrent DC electrokinetic transport of the particulate solution and DC/AC dielectrophoretic manipulation of the suspended particles [39–42]. This approach thus combines the advantages of DC and AC electrokinetics and offers independent controls of DC electrokinetic and AC dielectrophoretic motions [37, 38].

Classical electrophoresis deals with the motion of a particle in an unbounded stationary liquid subjected to a spatially uniform DC electric field [43, 44]. In microfluidic applications, however, the presence of a nearby channel wall may cause several influences on particle electrophoresis [45] through: (1) generating an electroosmotic flow of the suspending fluid due to the wall's nonzero charge [46]; (2) altering the drag force on the particle due to the wall's nonslip velocity [47]; (3) breaking the symmetry of the electric field distribution around the particle due to the wall's nonconducting nature [48] (which potentially leads to an electrical lift force [49]; see Section 3.1). There have been quite a number of theoretical studies of the wall-induced drag effect on the axial (i.e., streamwise) electrophoretic motion of particles in straight microchannels [50–61]. The predicted retardation of particle electrophoresis in the electroosmotic flow of fluids has been verified in two recent particle experiments [62, 63] though its extent is much weaker than that in a pressure-driven flow [23, 45]. For particles that move in close proximity to a channel wall, the presence of the wall has been demonstrated both theoretically [64–68] and experimentally [69, 70] to actually enhance the electrophoretic motion.

The aim of this article is to review the recent advances in DC and DC-biased AC electrokinetic manipulations of particles for microfluidic applications. Our focus is upon the cross-stream particle motions in the DC electroosmotic flow of fluids that enable the diverse DC or DC/AC control of particle transport in microchannels. Such transverse particle motions may be a result of the wall-induced electrical lift (see Section 3) and/or the insulating structure-induced dielectrophoretic force (see Sections 4 and 5). They are each a nonlinear particle motion and can be generated by both DC and AC electric fields. This article is organized as follows. Section 2 presents a brief background of the linear and nonlinear electrokinetic phenomena along with the fundamental formulae. Sections 3 to 5 review in order the works on electrokinetic particle manipulations in straight microchannels with uniform cross sections, straight microchannels with varying cross sections, and curved microchannels. Each of these three sections starts with a compact theoretical analysis of the relevant electrokinetic phenomena. Section 6 concludes the article with the perspectives of some potentially significant research directions in the field.

2 Background

2.1 Linear electrokinetic phenomena

When brought into contact with a polar liquid like water (or any aqueous buffer solutions), a solid object (e.g., a fused silica capillary, a PDMS microchannel, or a particle) often gets spontaneously charged leading to the formation of an electric double layer (EDL) adjacent to its surface [46]. The thickness of EDL is characterized by the inverse of the Debye–Hückel parameter, κ, (or simply the so-called Debye length, $\lambda_D = 1/\kappa$), which, for symmetric electrolytes, is defined as [46]:

$$\kappa = \sqrt{\frac{2z^2e^2cN_A}{\varepsilon k_B T}}. \tag{1}$$

In this definition, z is the ionic valence, e is the proton charge, c is the electrolyte molar concentration, N_A is the Avogadro constant, ε is the liquid permittivity, k_B is the Boltzmann's constant, and T is the liquid temperature. Therefore, the EDL thickness in 0.01 mM to 100 mM buffer solutions varies from the order of 100 nm to 1 nm, which is much smaller than the characteristic length scale of typical microfluidic channels (on the order of 10 μm) [25, 27].

If a DC electric field is applied tangential to the surface of the object, the free ions within the EDL respond to the field and move to the oppositely charged electrode. These moving ions drag the liquid along with them yielding a motion relative to the fixed object named electroosmosis [46]. Under the limit of thin EDL, the electroosmotic fluid velocity, $\mathbf{U}_{EO}$, has a plug-like profile and is given by:

$$\mathbf{U}_{EO} = -\frac{\varepsilon\zeta_w}{\eta}\mathbf{E} = \mu_{EO}\mathbf{E}, \tag{2}$$

where ζ_w is the zeta potential of the object surface, η is the liquid viscosity, $\mathbf{E}$ is the applied electric field vector, and $\mu_{eo} = -\varepsilon\zeta_w/\eta$ is the electroosmotic mobility. Therefore, electroosmotic flow experiences a much smaller fluid resistance and causes a much smaller sample dispersion than the traditional parabolic pressure-driven flow [71,72]. If the object is a free particle of radius, a, the electrostatic force on its surface charge generates a motion relative to the unbounded stationary liquid called electrophoresis [46], whose velocity, $\mathbf{U}_{EP}$, is written as:

$$\mathbf{U}_{EP} = f(\kappa a)\frac{\varepsilon\zeta_p}{\eta}\mathbf{E} = f(\kappa a)\,\mu_{EP}\mathbf{E}, \tag{3}$$

where $f(\kappa a)$ is Henry's function [73] that becomes 2/3 and 1 at infinitely small (i.e., thick EDL, under which Eq. (3) reduces to Hückel equation) and large (i.e., thin EDL, under which Eq. (3) reduces to Smoluchowski equation) values of κa, respectively [46], ζ_p is the zeta potential of the particle, and $\mu_{EP} = \varepsilon\zeta_p/\eta$ is the (Smoluchowski) electrophoretic mobility.

Fluid electroosmosis and particle electrophoresis often coexist in microchannels under the action of a DC electric field. They are both in-line with the direction of electric field and each has a magnitude *linearly* proportional to the electric field strength. Moreover, as they are both related to the direct conversion of *electric* energy into *kinetic* energy, fluid electroosmosis and particle electrophoresis are often combined into one term named (linear) electrokinetic motion in the microfluidics community [25,27,34], which, under the thin EDL limit (i.e., $\kappa a \gg 1$), is written as,

$$\mathbf{U}_{EK} = \frac{\varepsilon(\zeta_p - \zeta_w)}{\eta}\mathbf{E} = (\mu_{EO} + \mu_{EP})\mathbf{E} = \mu_{EK}\mathbf{E}, \tag{4}$$

where μ_{EK} is the electrokinetic mobility. It is important to note that the microchannel walls alter the drag force on particles because of their nonslip condition [23]. This boundary effect on particle electrophoresis has been studied in various microchannels as noted in Section 1. For example, Keh and Anderson [45] obtained the following formula for the electrophoretic velocity of particles travelling along the centerline of a cylindrical pore:

$$\mathbf{U}_p = [1 - 0.28987\lambda^3 + 1.89632\lambda^5 - 1.02780\lambda^6 + O(\lambda^8)] \times \frac{\varepsilon\left(\zeta_p - \zeta_w\right)}{\eta}\mathbf{E}, \tag{5}$$

where $\lambda = a/R$ is the particle confinement ratio with a and R being the radii of the particle and pore, respectively. This predicted wall-retardation effect (see the terms in the square brackets) is typically small unless $\lambda \sim O(1)$ [45]. It is therefore often safe to use the simple formula in Eq. (4) to obtain a particle's electrokinetic velocity (or mobility) in any microchannels without drawing significant errors.

2.2 Nonlinear electrokinetic phenomena

Nonlinear electrokinetic phenomena refer to those electrically driven fluid flows or particle motions that depend *nonlinearly* on the applied electric field strength [74]. Three types of nonlinear electrokinetic phenomena are typically involved in DC electrokinetic manipulation of particles in microchannels, which are dielectrophoretic particle motion, electrothermal fluid flow, and induced charge electroosmotic fluid flow [74, 75]. These phenomena are briefly reviewed below with the focus on particle DEP because the two fluid flows are usually rendered weak in electrokinetic microfluidic devices in order to minimize the adverse impacts on the samples and devices and as well ensure the accuracy in particle transport and placement [37, 38]. The review of the recent studies on nonlinear fluid flows in electric field-mediated microfluidic devices will be deferred to a future article.

DEP is the motion of a particle, regardless of surface charge, in response to a nonuniform electric field (either DC or AC) as a result of the difference in polarizability between the particle and the suspending fluid [28]. Since its discovery 50 years ago [76], DEP has become a powerful tool in manipulating various micro/nano-sized particles due to its high sensitivity [77–81]. It has thus far been implemented in primarily two forms: the traditional electrode-based DEP (eDEP) [82–85] and the emerging iDEP [86–89]. In eDEP microdevices, pairs of microelectrodes are patterned inside a microchannel, upon which high-frequency AC voltages are imposed to achieve locally strong electric field gradients. In contrast, iDEP microdevices utilize in-channel insulating microstructures to block electric current for the generation of locally nonuniform electric fields [90–93]. Both DC and DC-biased AC electric fields can be used in iDEP devices [37, 38, 88, 89]. Depending on if they are more or less polarizable than the suspending fluid, particles migrate either along (i.e., positive DEP or pDEP) or against (i.e., negative DEP or nDEP) the electric field gradients [28] with a dielectrophoretic velocity, $\mathbf{U}_{DEP}$, which, for spherical particles under the point-dipole approximation [29], is given by:

$$\mathbf{U}_{DEP} = \frac{a^2\varepsilon}{3\eta}\mathrm{Re}\{f_{CM}\}\nabla\mathbf{E}^2, \tag{6}$$

$$f_{CM} = \frac{\varepsilon_p^* - \varepsilon^*}{\varepsilon_p^* + 2\varepsilon^*}, \tag{7}$$

where $\mathrm{Re}\{f_{CM}\}$ denotes the real part of the complex Clausius−Mossotti (CM) factor, $\varepsilon_p^* = \varepsilon_p - j\sigma_p/\omega$ and $\varepsilon^* = \varepsilon - j\sigma/\omega$ are the complex permittivity of the particle and fluid, respectively, with ε_p being the particle permittivity, σ_p the particle conductivity, $j = \sqrt{-1}$, ω the angular frequency of the electric field, and σ the fluid conductivity. In both DC

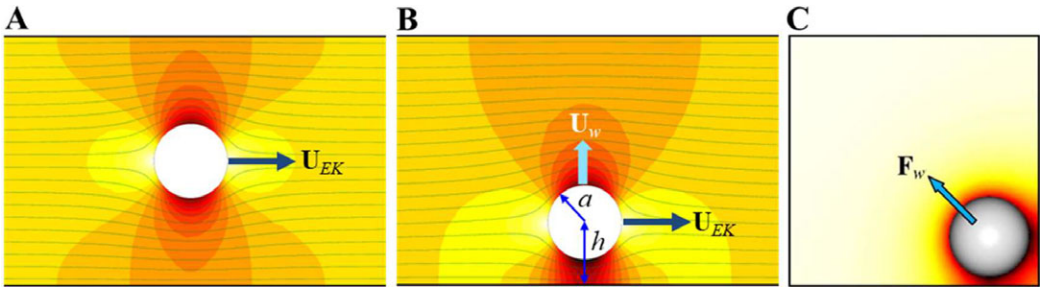

Figure 1. Electric field contour (the darker color, the larger magnitude) and lines around a spherical particle in the horizontal plane of a straight microchannel when the electrophoretic motion is along (A) and off (B) the centerline at an electrokinetic velocity, $\mathbf{U}_{EK}$. The particle in (B) drifts away from the lower channel wall at a velocity, $\mathbf{U}_w$, because of a wall-induced electrical lift, $\mathbf{F}_w$, that arises from the asymmetric electric field about itself. Adapted with permission from Lu et al. [144], © 2015 American Chemical Society. (C) shows the electric field contour around an off-center particle in the cross section of a straight square microchannel. Adapted with permission from Liang et al. [140], © 2010 Elsevier.

and DC-biased AC (where the AC field frequency is normally limited to a few tens of kHz because of the low slew rate of high-voltage amplifiers) electrokinetic manipulations, the CM factor is mainly determined by the electric conductivities of the fluid and particle, that is:

$$f_{CM} = \frac{\sigma_p - \sigma}{\sigma_p + 2\sigma}. \tag{8}$$

The electric conductivity of dielectric (e.g., polystyrene) particles is usually much smaller than that of the suspending fluid. For biological particles (e.g., cells), the applied electric potential is dropped primarily across the cellular membrane in low-frequency electric fields [26]. Therefore, the electric conductivity of cells in DC and DC-biased AC electrokinetic manipulations mainly depends on the conductivity of their membranes, which has been reported to be on the order of 10^{-3} μS/cm and 10 μS/cm for viable and nonviable cells, respectively [85, 90–92]. As both values are much smaller than the conductivity of typical buffer solutions, it is often safe to assume $f_{CM} = -0.5$ for dielectric particles and cells in microfluidic applications. Thus, Eq. (6) is reduced to:

$$\mathbf{U}_{DEP} = -\frac{a^2\varepsilon}{6\eta}\nabla\mathbf{E}^2 = \mu_{DEP}\nabla\mathbf{E}^2, \tag{9}$$

which indicates an nDEP toward the low electric field region [28–30] with $\mu_{DEP} = -a^2\varepsilon/6\eta$ being the (negative) dielectrophoretic particle mobility.

Electrothermal flow is the fluid motion caused by Joule heating effects because of the action of electric field on the thermally induced fluid property gradients [94–96]. This flow often manifests itself in the form of counter-rotating vortices if the electric field or the fluid electric conductivity is sufficiently high [97, 98]. It scales as a 4th-order function of the applied electric field [99], which has been exploited to mix samples [100] for enhanced biochemical sensing. However, Joule heating effects and the induced electrothermal fluid flow have also been demonstrated to weaken the dielectrophoretic focusing and trapping of microparticles [101–104]. Induced charge electroosmotic flow is the fluid motion caused by the action of electric field on the diffuse charge produced on an electrically polarizable (either conducting or dielectric) surface [105, 106]. This flow has a nonlinear quadratic dependence on the electric field and often consists of two counter-rotating rolls [107–109]. It has been extensively studied around conducting surfaces (e.g., metal electrodes and particles) that can be either electrically activated [110–113] or left floating [114–117]. Induced charge electroosmotic fluid flow also takes place around inert objects with sharp edges (e.g., acute corners) because of the electric field leakage [118–123], which has been demonstrated to disturb the local fluid flow and particle motion [124, 125].

3 Straight microchannels with uniform cross sections

3.1 Theoretical analysis

In a straight microchannel with a constant cross section, electric field lines pass uniformly through a homogeneous fluid parallel to the walls, leading to a plug-like electroosmotic flow under the thin EDL limit because of the similarity of the electric and velocity fields [126]. However, the presence of a dielectric particle inside the microchannel can cause distortions to the electric field lines (and as well the fluid streamlines) as long as it has dissimilar electrical properties from the suspending fluid. As viewed from its contour in Fig. 1A, the electric field is symmetric about the particle in both the axial and transverse directions for the case of particle electrophoresis along the channel axis. Therefore, the total electrical force acting on the particle, which is the surface integral of the Maxwell stress tensor [36, 48], should be zero. In contrast, for off-center particle electrophoresis, the electric field distribution becomes asymmetric in the transverse direction as demonstrated in Fig. 1B. This leads to a dielectrophoretic-like force, $\mathbf{F}_w$ (see Fig. 1C), which causes the particle to drift away from the nearby wall(s). Such a wall-induced electrical lift was first considered by Young and Li [127] in their theoretical model to counterbalance the gravity of an electrophoretically moving particle near a plane wall. It was later analyzed by several other research groups to account for the effects

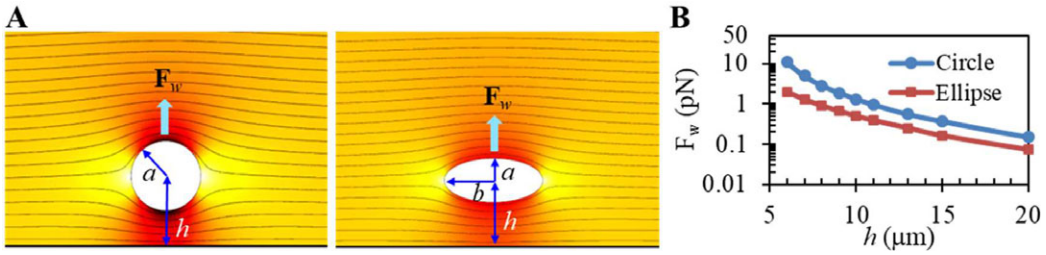

Figure 2. Particle shape effect on the wall-induced electrical lift. (A) Compares the electric field lines and contours (the darker color, the larger magnitude) around a circular particle (left, $a = 5$ μm) and an elliptical particle (right, $a = 10/3$ μm and $b = 7.5$ μm) of equal area when they travel electrophoretically through a 100 μm wide straight slit microchannel with an identical $h = 10$ μm particle center-wall distance. (B) Compares the wall-induced electrical lift forces (computed in COMSOL® using the surface integral of the Maxwell stress tensor), $\mathbf{F}_w$, on the two equal-area particles versus the particle center-wall distance, h.

of particle–wall interactions on particle electrophoresis and DEP [70, 128–132]. The existence of this electrical lift was experimentally verified by Yoda's group [133, 134] through the use of evanescent wave-based particle-tracking velocimetry.

The wall-induced lateral migration velocity, $\mathbf{U}_w$, in particle electrophoresis parallel to a plane dielectric wall has been recently proposed by Yariv [49, 135] to take the following form at the leading order:

$$\mathbf{U}_w = f(Du)\,\frac{\varepsilon a E^2}{32\eta}\left(\frac{a}{h}\right)^4 \mathbf{n}, \tag{10}$$

where h is the normal distance of the spherical particle center to the wall (see Fig. 1B), $\mathbf{n}$ is the unit normal vector of the wall that points into the fluid, and $f(Du)$ is a dimensionless factor to account for the surface conduction effect in terms of the Dukhin number [136], Du:

$$Du = \frac{2}{\kappa a}(1+2\alpha)\left[\cosh\left(\frac{ze\zeta_p}{2k_BT}\right)-1\right]\left(1+\frac{K^{\sigma i}}{K^{\sigma d}}\right). \tag{11}$$

In the above equation, $K^{\sigma i}$ is the surface conductivity due to the stagnant layer charge, $K^{\sigma d}$ is the surface conductivity due to the diffuse layer charge, and:

$$\alpha = (\varepsilon/\eta D)\,(k_BT/ze)^2, \tag{12}$$

which is a dimensionless number [137] with D being the (assumed) equal cationic and anionic diffusivity. Therefore, Du is a function of particle charge (ζ_p) and fluid molar concentration (κ) as well as other fluid properties involved in α. Apparently, the wall-induced lateral particle migration, $\mathbf{U}_w$ in Eq. (10), in electroosmotic flow through straight uniform microchannels is another nonlinear electrokinetic phenomenon because of its quadratic dependence on the applied electric field (can hence be induced in both DC and AC electric fields). It is important to note that Eq. (10) is only valid for remote particle–wall interactions, that is, $a/h \ll 1$. Moreover, the contribution of hydrodynamic lift to $\mathbf{U}_w$ has been ignored because of the negligible inertial effect in typical electrokinetic flows [24, 25, 27].

The competition of $\mathbf{U}_{EK}$ in Eq. (4) and $\mathbf{U}_w$ in Eq. (10) results in a particle deflection across the fluid streamlines during a travelling length, L,

$$deflection = \frac{U_w L}{U_{EK}} = f(Du)\,\frac{a}{32}\left(\frac{a}{h}\right)^4 \frac{LE}{\zeta_p - \zeta_w}, \tag{13}$$

which is a function of both particle size (a) and charge (ζ_p). The $deflection$ is also a function of particle shape (and hence potentially particle stiffness) because of the dependence of the wall-induced electrical lift, $\mathbf{F}_w$, on the particle aspect ratio, $AR_p = b/a$, where a and b are the semi-minor and semi-major axes of an ellipse. This is illustrated by the dissimilar electric field distributions around a 2D elliptical particle ($a = 10/3$ μm and $b = 7.5$ μm) and an equal-area circular particle ($a = 5$ μm) in Fig. 2A (note: the major axis of the elliptical particle is assumed to align with the electric field, that is, parallel to the channel walls [138]). It is further verified by comparing the computed $\mathbf{F}_w$ on these two particles in a 100 μm wide straight microchannel with an identical particle center-wall distance, h, under a 400 V/cm DC electric field. As seen from the line plot in Fig. 2B, $\mathbf{F}_w$ on the circular particle is always larger than that on the elliptical particle and nearly five times the latter at small h values. This relationship remains also valid for the two particles even with the same particle edge-wall distance, that is, $h - a$. We believe that the difference in $\mathbf{F}_w$ between a spherical particle and a spheroidal particle of equal volume in a real 3D microchannel should be even greater than that shown in Fig. 2B. Moreover, as the sphere experiences a smaller drag force than the spheroid [47], $\mathbf{F}_w$ should deflect the former particle away from the wall at a higher rate. The dependence of $deflection$ on particle size, charge, and shape enables a label-free separation of particles by any of these physical properties.

It is important to note that the axial electrokinetic particle motion, $\mathbf{U}_{EK}$ in Eq. (4), is driven by DC electric field only. In contrast, the wall-induced lateral particle migration, $\mathbf{U}_w$ in Eq. (10), can be generated by both DC and AC fields due to its 2nd order dependence of electric field. Therefore, if a DC-biased AC electric field is applied across a straight uniform microchannel, the resulting $deflection$ (see Eq. (13)) for

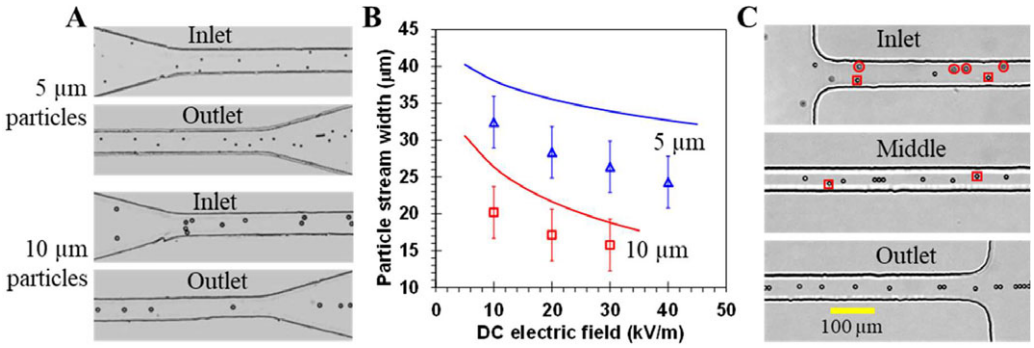

Figure 3. Electrokinetic focusing of particles in straight rectangular microchannels via the wall-induced electrical lift. (A) Shows the top-view snapshot images of 5 and 10 μm diameter spherical polystyrene particles in 1 mM phosphate buffer through a 50 μm wide, 25 μm deep straight microchannel under a 300 V/cm (or 30 kV/m) DC electric field. (B) Compares the experimentally measured (symbols with error bars) and theoretically predicted (lines) widths of the focused particle streams at the channel outlet under various DC electric fields. Adapted with permission from Liang et al. [139], © 2010 Elsevier (C) Shows the top-view snapshot images of 10 μm particles in a density-matched glycerol-buffer solution at the inlet, middle, and outlet of a 50 μm × 50 μm straight square microchannel under a 200 V/cm DC electric field, where, for clarity, the off-centered and defocused particles are highlighted with squares and circles, respectively. Adapted with permission from Liang et al. [140], © 2010 Elsevier.

particles with negligible surface conduction effects is written as:

$$deflection = \left(1 + r^2\right) \frac{a}{32} \left(\frac{a}{h}\right)^4 \frac{L E_{DC}}{\zeta_p - \zeta_w}, \tag{14}$$

where r is the AC (root-mean-square value) to DC field ratio with E_{DC} being the DC field strength. This revised equation indicates a significantly enhanced electrical lift effect at an increasing value of r, wherein the particle throughput can still remain unvaried if the DC field component is maintained. In other words, it is principally possible to use the wall-induced electrical lift to control the motion of small (e.g., submicron or even nanoscale) particles in microchannels as long as the particle confinement ratio is not small.

3.2 Electrokinetic focusing of particles

The first direct demonstration of the consequence of wall-induced electrical lift was reported by Liang et al. [139]. As the equilibrium position of particles lies in the center of the channel cross section (see Fig. 1C), the electrical lift, $\mathbf{F}_w$, can produce an automatic focusing effect on particles in both the horizontal and vertical planes of the microchannel. As illustrated by the top-view images in Fig. 3A, both 5 and 10 μm diameter spherical polystyrene particles in 1 mM phosphate buffer travel into a 50 μm wide, 25 μm deep straight microchannel uniformly over the width, while exiting it in a centrally focused stream under a 300 V/cm DC electric field. Moreover, 10 μm particles obtain an apparently better focusing than 5 μm ones because of the particle size-dependence of the wall-induced lateral $deflection$ in Eq. (13). Figure 3B shows a quantitative comparison of the experimentally measured and theoretically predicted widths of the focused particle streams. It is obvious that Eq. (10) (with $f(Du) = 1$) significantly underpredicts the wall-induced electrical lift effect through it does predict correctly the trend of enhanced focusing with increasing electric field for both sizes of particles. Liang et al. [140] also demonstrated a 3D focusing of 10 μm particles in the electroosmotic flow of a density-matched glycerol-buffer solution. As the focal plane of the microscope objective was positioned to the middle of the channel depth, any off-centered (in the channel width direction) or defocused (in the channel depth direction) particles can be clearly identified. All particles move out of the microchannel in a single file in Fig. 3C.

Later, Liu et al. [141] studied how the ionic concentration of the suspending fluid affects the wall-induced DC electrokinetic focusing of 5 μm polystyrene particles in the same 50 μm by 25 μm straight rectangular microchannel (Fig. 4A). At the inlet of the microchannel, particles are randomly and uniformly distributed over the channel width in all solutions. They are directed toward the channel centerline by the wall-induced electrical lift, leading to an apparently enhanced focusing effect at the outlet with decreasing buffer concentration (or accordingly increasing Dukhin number, Du, in Eq. (11)). As the measured electrokinetic particle mobility increases approximately logarithmically with decreasing buffer solution [142], the observed phenomenon in Fig. 4A should result from the substantially increased electrical lift. This may be associated with the surface conduction effect in terms of Du as reflected by the factor, $f(Du)$, in Eq. (10). Liu et al. [143] further studied the wall-induced electrokinetic focusing of four types of 10 μm diameter polystyrene particles from Sigma, Bangs, Thermo, and Duke, respectively, in 1 mM phosphate buffer through the same straight rectangular microchannel under varying DC electric fields (Fig. 4B). Sigma particles apparently migrate toward the channel centerline exhibiting the strongest electrokinetic focusing. Next to them are the Bangs, Thermo, and Duke particles in order, among which the last one experiences little focusing effect even at the highest electric field in our tests. Interestingly, Sigma particles were found to move the fastest, ahead of Bangs, Thermo, and Duke particles in the order of decreasing velocity. In other

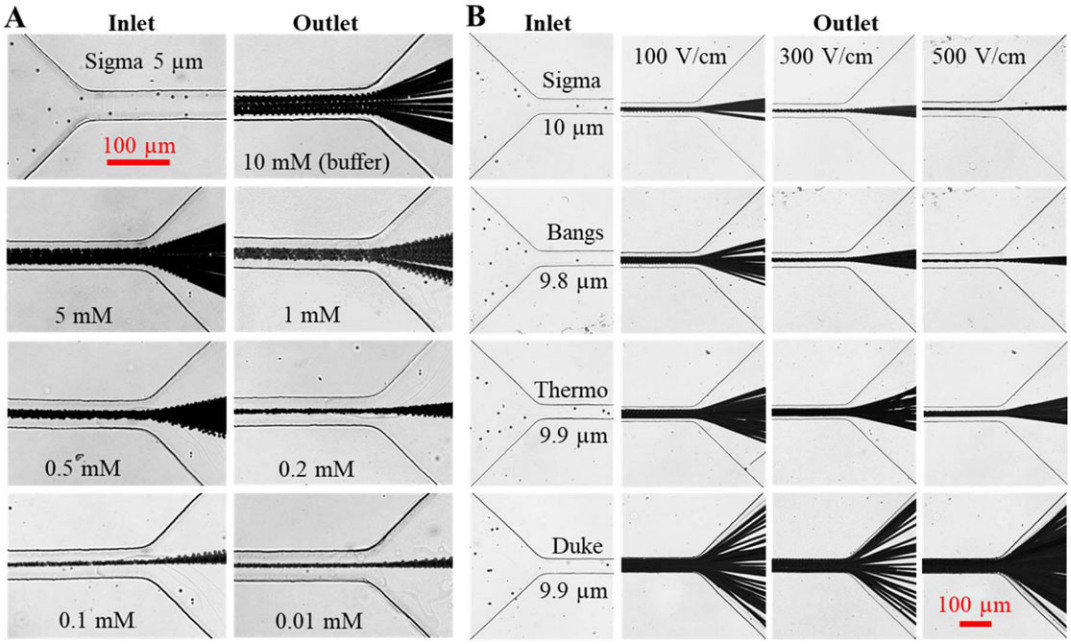

Figure 4. Parametric effects on wall-induced electrokinetic centerline focusing of particles in straight rectangular microchannels. (A) Top-view images illustrating the surface-conduction enhanced focusing of 5 μm diameter polystyrene particles in the flow of buffer solutions of varying molar concentrations through a 50 μm wide, 25 μm deep straight rectangular microchannel under a fixed 300 V/cm DC electric field. Adapted with permission from Liu et al. [141], © 2017 American Institute of Physics. (B) Top-view images showing the electrokinetic focusing of 10 μm diameter Sigma, Bangs, Thermo, and Duke particles in the flow of 1-mM phosphate buffer solution through a 50 μm wide and 25 μm deep straight rectangular microchannel under varying DC electric fields. Adapted with permission from Liu et al. [143], © 2019 Wiley-VCH.

words, the faster the particle moves, the better electrokinetic focusing is achieved. This phenomenon appears analogous to the enhanced electrokinetic focusing of Sigma particles in buffers of decreasing concentrations (Fig. 4A). The reason behind these observations needs further studies.

3.3 Electrokinetic separation of particles

The wall-induced particle property-dependent *deflection* in Eq. (13) has also been exploited to achieve label-free electrokinetic separations of particles in straight rectangular microchannels. Lu et al. [144] demonstrated a continuous sheath-flow separation of 5 and 10 μm diameter polystyrene particles in the DC electroosmotic flow of 1 mM buffer solution through a T-shaped microchannel (Fig. 5A). The main branch of this channel is 200 μm wide, much larger than the particle size. The particle mixture is prefocused by a particle-free sheath flow to a stream near the upper sidewall of the main-branch, which is then gradually split into two sub-streams under an average DC electric field of around 500 V/cm because of the particle-size-dependent *deflection*. The whole process is reasonably simulated by tracking the particle trajectories using Eq. (4) for $\mathbf{U}_{EK}$ and Eq. (10) for $\mathbf{U}_w$ via a Lagrangian Tracking Method (LTM). Li et al. [145] later revised this wall-induced electrokinetic separation by the use of a bifurcating microchannel with a uniform rectangular cross section to eliminate the sheath flow-focusing of particles. Figure 5B shows the experimental and numerical results for such a sheath-free separation at several locations of the microchannel. The wall-induced electrical lift first focuses 5 and 15 μm particles toward the centerline of the 65 μm wide main-branch under an average DC electric field of around 500 V/cm, and then deflects them to size-dependent flow paths in each side-branch.

Thomas et al. [146] demonstrated a sheath-flow separation of yeast cells from 5 μm polystyrene particles by charge in the electroosmotic flow of a density-matched phosphate buffer/glycerol solution through a ψ-shaped microchannel (Fig. 6, upper panel) via the wall-induced electrical lift. The average electric field in the main-branch is around 180 V/cm. The particles and yeast cells in the mixture are both well focused at the trifurcation. However, yeast cells experience a greater deflection than the similar-sized particles in the main-branch because of the greater electrokinetic mobility of the latter, leading to a separation at the outlet expansion (Fig. 6, lower left panel). As demonstrated by the probability distribution function plot in Fig. 6 (lower right panel), the separation efficiency and purity for yeast cells inside the core region are 83 and 94% while those for particles outside the core region are both 100%. In another study, Li and Li [147] demonstrated a sheath-flow separation of 50 μm diameter oil and Janus droplets in an X-shaped microchannel. The authors assumed no deformations of either type of droplets under an electric field, leading to an equal magnitude for the wall-induced electrical lift. However, as they have a larger

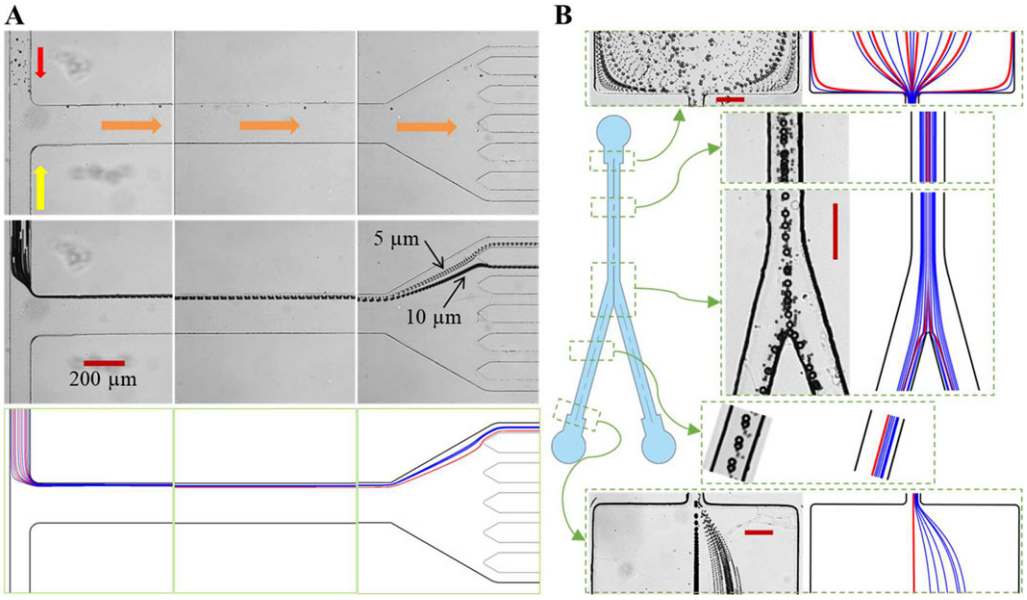

Figure 5. Electrokinetic separation of spherical polystyrene particles by size via the wall-induced electrical lift in straight rectangular microchannels. (A) Sheath-flow separation of 5 and 10 μm diameter particles in a T-shaped microchannel under an average 500 V/cm DC electric field in the 200 μm wide main branch (top row, snapshot images; middle row, superimposed image; bottom row, theoretically predicted trajectories). Adapted with permission from Lu et al. [144], © 2015 American Chemical Society. (B) Experimental and numerical results for a sheath-free separation of 5 and 15 μm diameter particles in a 65 μm wide and 40 μm deep bifurcating microchannel under an average 500 V/cm DC electric field (left panel at each location, superimposed image; right panel at each location, predicted trajectories). Adapted with permission from Li et al. [145], © 2016 American Institute of Physics.

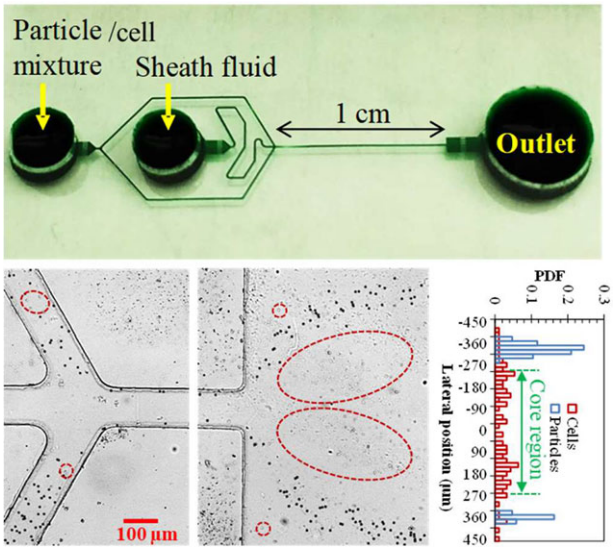

Figure 6. Sheath-flow electrokinetic separation of yeast cells and 5 μm polystyrene particles by charge in 1 mM phosphate buffer/glycerol solution through a ψ-shaped rectangular microchannel (upper panel) under an average DC electric field of 180 V/cm. The lower left panel shows the experimental images (cells are highlighted by the circles) at the trifurcation and outlet expansion, respectively, and the lower right panel shows the probability distribution function plot for cells and particles. Adapted with permission from Thomas et al. [146], © 2017 Wiley-VCH.

electrokinetic mobility than oil droplets, Janus droplets experience a smaller electrical *deflection* in the 250 μm wide main-branch of the channel. The authors also demonstrated a size-based separation of Janus and oil droplets, respectively, in the same microchannel.

4 Straight microchannels with varying cross sections

4.1 Theoretical analysis

In a straight microchannel with varying cross sections, electric field becomes inherently nonuniform because of the continuity of electric current. Figure 7A shows the contour of electric field at a microchannel constriction, where the local electric field magnitude increases significantly from the microchannel to the constriction. Hence, particles experience a dielectrophoretic force, $\mathbf{F}_{DEP}$, when travelling into the constriction. As noted earlier, this force usually directs particles toward the low electric field region in typical buffer solutions [26, 37, 38], which is illustrated by the arrows of $\mathbf{F}_{DEP}$ in Fig. 7B. The resulting negative dielectrophoretic motion, $\mathbf{U}_{DEP}$, therefore points outward from the channel constriction. Essentially, there exist two sources for electric field nonuniformities at the constriction region. One source is the reduced cross sectional area from the microchannel to the constriction, which causes electric field gradients primarily along the direction of electric field lines (see Fig. 7C).

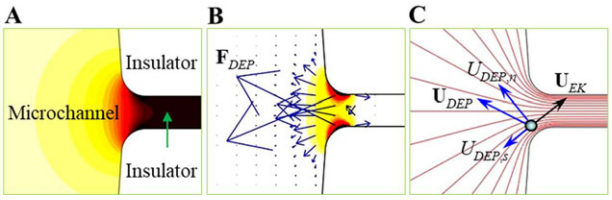

Figure 7. Electric field-induced particle DEP at a microchannel constriction: (A) Contour (the darker the larger) of electric field; (B) Arrows (length proportional to the magnitude) and contour (the darker the larger) of the dielectrophoretic force, $\mathbf{F}_{DEP}$; (C) Particle velocity analysis (background shows the electric field lines or equivalently the fluid streamlines in the absence of the particle [126]), where $\mathbf{U}_{DEP}$ (broken down into $U_{DEP,s}$ and $U_{DEP,n}$ along and normal to the streamline, respectively) and $\mathbf{U}_{EK}$ are the dielectrophoretic and electrokinetic velocities. Adapted with permission from Zhu et al. [149], © 2012 Wiley-VCH.

The other source is the discrepancy in path length for electric current around the corners of the constriction (see also Section 5.1), which causes electric field gradients mainly normal to the direction of electric field lines. Considering the fact that the electric field lines are equivalent to fluid streamlines in pure electrokinetic flows [126], one may conveniently break down $\mathbf{U}_{DEP}$ in Eq. (9) based on the streamline coordinates:

$$U_{DEP} = U_{DEP,s}\hat{s} + U_{DEP,n}\hat{n} = \mu_{DEP}\left(\frac{\partial E^2}{\partial s}\hat{s} + 2\frac{E^2}{\Re}\hat{n}\right), \quad (15)$$

where $U_{DEP,s}$ is the dielectrophoretic velocity component in the streamline direction with the unit vector $\hat{\mathbf{s}}$, $U_{DEP,n}$ is the dielectrophoretic velocity component normal to the streamline direction with the unit vector $\hat{\mathbf{n}}$, and $\Re$ is the radius of curvature of the streamline. For the case of DC-biased AC electric fields, Eq. (15) can be rewritten as:

$$\mathbf{U}_{DEP} = (1+r^2)\mu_{DEP}\nabla\mathbf{E}_{DC}^2 = (1+r^2)\mu_{DEP}\left(\frac{\partial \mathbf{E}_{DC}^2}{\partial s}\hat{\mathbf{s}} + 2\frac{\mathbf{E}_{DC}^2}{\Re}\hat{\mathbf{n}}\right). \quad (16)$$

As viewed from the particle velocity analysis in Fig. 7C, the cross-stream dielectrophoretic motion, $U_{DEP,n}$, points toward the centerline of the microchannel, yielding a *deflection* similar to that defined in Eq. (14) for the wall-induced lateral particle migration and in turn a particle focusing effect. The effectiveness of this action is determined by the ratio of $U_{DEP,n}$ to the particle velocity in the streamline direction, that is,

$$\left|\frac{U_{DEP,n}}{U_{EK}+U_{DEP,s}}\right| = \frac{2(1+r^2)\frac{E_{DC}}{\Re}}{\left|\frac{\mu_{EK}}{\mu_{DEP}}\right| - 2(1+r^2)\frac{\partial E_{DC}}{\partial s}}. \quad (17)$$

Such a DEP-based particle deflection/focusing can be enhanced by increasing the value of r or E_{DC} and as well decreasing the constriction-to-channel width ratio or the corner radius of the constriction. Further, as the streamwise dielectrophoretic motion, $U_{DEP,s}$, is against the electrokinetic motion, U_{EK}, particles are dielectrophoretically slowed down at the microchannel constriction. Moreover, since $U_{DEP,s}$ (as a nonlinear phenomenon) has a greater dependence on electric field than U_{EK} (as a linear phenomenon), one can expect the incoming particles to be stagnated in front of the constriction when the DC and/or AC electric field increases. The threshold DC electric field, E_{th_DC}, for such a dielectrophoretic trapping of particles is given by:

$$\frac{\partial E_{th\_DC}}{\partial s} = \frac{1}{2(1+r^2)}\left|\frac{\mu_{EK}}{\mu_{DEP}}\right|. \quad (18)$$

It is evident that the DEP-based particle deflection/focusing and trapping at a microchannel constriction are each a strong function of the particle mobility ratio:

$$\frac{\mu_{EK}}{\mu_{DEP}} = \frac{6(\zeta_p - \zeta_w)}{a^2}, \quad (19)$$

which can be utilized to separate particles by size or surface charge. Moreover, similar to the particle shape dependence of the wall-induced electrical lift in Section 3.1, the dielectrophoretic mobility, μ_{DEP}, in Eq. (19) is also a function of particle shape enabling potentially a shape-based particle separation by DEP (see further analysis in Section 5.1).

4.2 From reservoir to microchannel

The significant size-mismatch between a macro reservoir (usually a few millimeters in diameter) and a microchannel (usually a few tens microns in the cross section) causes inherent electric field gradients at the reservoir-microchannel junction. Thus induced dielectrophoretic motion has been recently exploited by the author's group to focus, trap, and separate various particles. The first demonstration of such a reservoir-based DEP (rDEP) technique [148] was reported by Zhu et al. [149]. Figure 8A shows the experimental images of 3 μm polystyrene particles in the electroosmotic flow of 1 mM phosphate buffer through the reservoir-microchannel junction of an end-tapered straight rectangular microchannel (Fig. 8B). The average DC electric field across the channel is fixed at 50 V/cm. With the increase of the AC to DC field ratio, r, particles undergo a process starting from a uniform transport across the channel width ($r = 0$), to a depletion from either channel walls ($4 \le r \le 9$), then a single-file focusing along the channel center ($r = 13$), and finally a continuous trapping right before the junction ($r = 19$). This whole process is reasonably simulated by a 2D LTM-based numerical model in COMSOL®, where the particle velocity is given by

$$\mathbf{U}_p = \mu_{EK}\mathbf{E}_{DC} - c(1+r^2)\mu_{DEP}\nabla\mathbf{E}_{DC}^2.$$

In this equation, a correction factor, $c = 0.6$, was introduced to account for the particle size effect on dielectrophoretic velocity [128]. Figure 8C shows the experimental and numerical results for a selective concentration and separation of 3 μm particles from 1 μm particles at the reservoir-microchannel junction via rDEP under a 50 V/cm DC/950 V/cm AC electric field (i.e., $r = 19$). The two types of particles have an equal electrokinetic mobility. Hence,

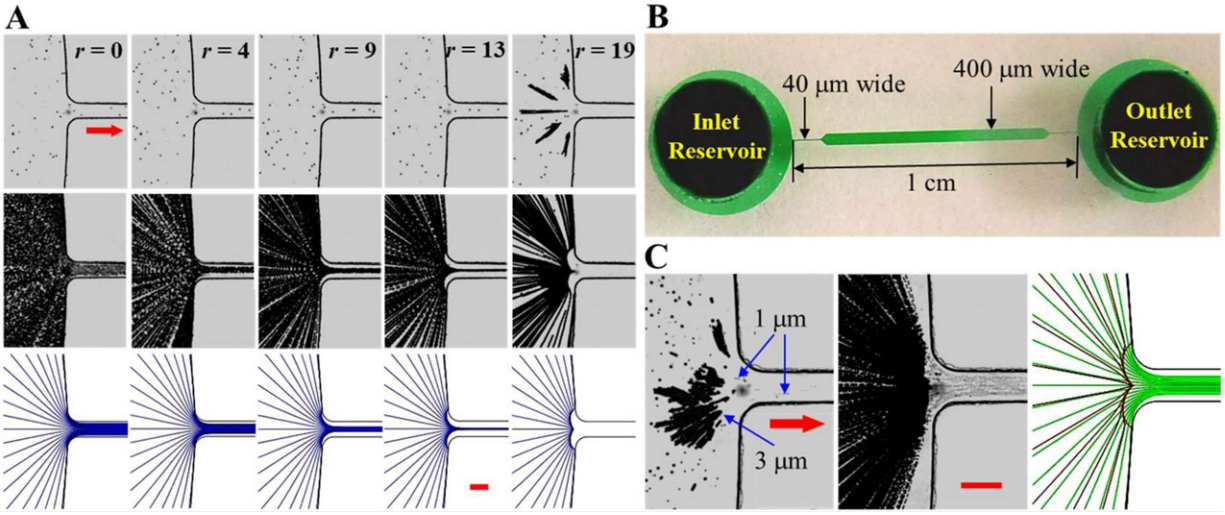

Figure 8. Particle focusing, trapping, and separation (by size) via rDEP at the reservoir-microchannel junction. (A) Comparison of experimentally obtained images and numerically predicted trajectories of 3 μm diameter polystyrene particles in 1 mM phosphate buffer solution under various 50 V/cm DC-biased AC electric fields (reflected by the AC to DC field ratio, *r*). (B) Top-view image of the straight rectangular microchannel with a tapered section at each end. (C) Selective concentration and separation of 3 μm particles from 1 μm particles (left, snapshot image; middle, superimposed image; right, predicted particle trajectories) under the electric field of 50 V/cm DC/950 V/cm AC (i.e., $r = 19$). Adapted with permission from Zhu et al. [149], © 2012 Wiley-VCH.

3 μm particles bear a smaller mobility ratio, μ_{EK}/μ_{DEP} in Eq. (19), leading to a lower threshold electric field, $\mathbf{E}_{th\_DC}$ in Eq. (18), for dielectrophoretic trapping than 1 μm particles. Such a size-based rDEP separation of particles was later improved by the use of parallel microchannels in a stacked device [150] and 3D reservoir-microchannel junction [151], respectively.

Later, Patel et al. [152] implemented a surface charge-based separation of 3 μm fluorescent and plain particles in 0.1 mM phosphate buffer using rDEP under an average electric field of 40 V/cm DC/640 V/cm AC (Fig. 9A). Fluorescent particles are concentrated inside the reservoir while the plain particles can pass through the junction in a focused stream along the centerline of the microchannel. This separation is a result of the smaller electrokinetic mobility of the fluorescent particles, such that they possess a smaller mobility ratio, μ_{EK}/μ_{DEP}, and hence can be trapped more easily than the equal-sized plain particles. Moreover, the streak images of the two types of particles during the separation process agree reasonably with the predicted trajectories from a LTM-based 2D model. Patel et al. [153] further demonstrated a viability-based separation of live and dead yeast cells in 1 mM phosphate buffer at a reservoir-microchannel junction (Fig. 9B). The nonfluorescent dead yeasts are trapped and enriched inside the reservoir while the fluorescent live yeasts can travel through the microchannel. This rDEP-based separation results from two impacts when yeast cells lose viability. One is the decreased conductivity in the nucleus and the increased conductivity in the membrane [154], which alters the CM factor of DEP in Eq. (7) [26, 85]. The other impact lies in the reduced electrokinetic mobility, which along with the CM factor causes a decrease in the cell mobility ratio, μ_{EK}/μ_{DEP}, and hence an easier trapping for dead cells. Such a selective concentration and separation of live and dead yeast cells is also reasonably simulated by a LTM-based model.

4.3 One-dimensional widthwise in-channel variations

There have been several dozens of papers published on DC (or DC-biased AC) electrokinetic manipulation of particles in straight microchannels with one or multiple variations in the width direction of the cross section [37, 38]. These 2D widthwise constrictions, which span the whole channel depth, can be formed by patterning either insulating hurdles on the sidewalls (Figs. 10 and 11) or insulating posts on the bottom walls (Fig. 12) of microchannels through, for example, a simple single-layer soft lithography technique. We review the works in each of these structures in separate sections below.

4.3.1 Insulating hurdles patterned on the sidewalls of microchannels

Xuan et al. [155] studied the accelerated particle motion in the DC electroosmotic flow of water through converging-diverging microchannels. They found that the ratio of particle velocity in the 55 μm wide throat to that in the 325 μm wide straight channel is significantly lower than the cross sectional area ratio and dependent on particle size (Fig. 10A). They attributed this phenomenon to the negative dielectrophoretic force induced in the throat region, which was later verified by a numerical simulation from Ai et al. [156]. Xuan et al. [63] also observed a strong dielectrophoretic focusing of 40 μm

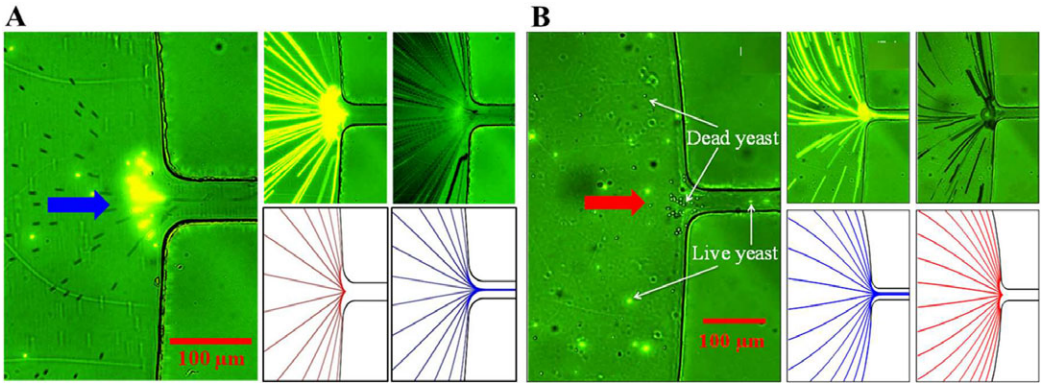

Figure 9. Particle separation by nonsize properties via rDEP at the reservoir-microchannel junction. (A) Surface charge-based separation of 3 μm diameter fluorescent and plain polystyrene particles under an average 40 V/cm DC/640 V/cm AC electric field. Adapted with permission from Patel et al. [152], © 2013 Wiley-VCH. (B) Viability-based separation of live (fluorescent) and dead (nonfluorescent, appearing as dark hollow circles due to optical reflections) yeast cells under an average 12 V/cm DC-biased 140 V/cm AC electric field. Adapted with permission from Patel et al. [153], © 2012 American Institute of Physics.

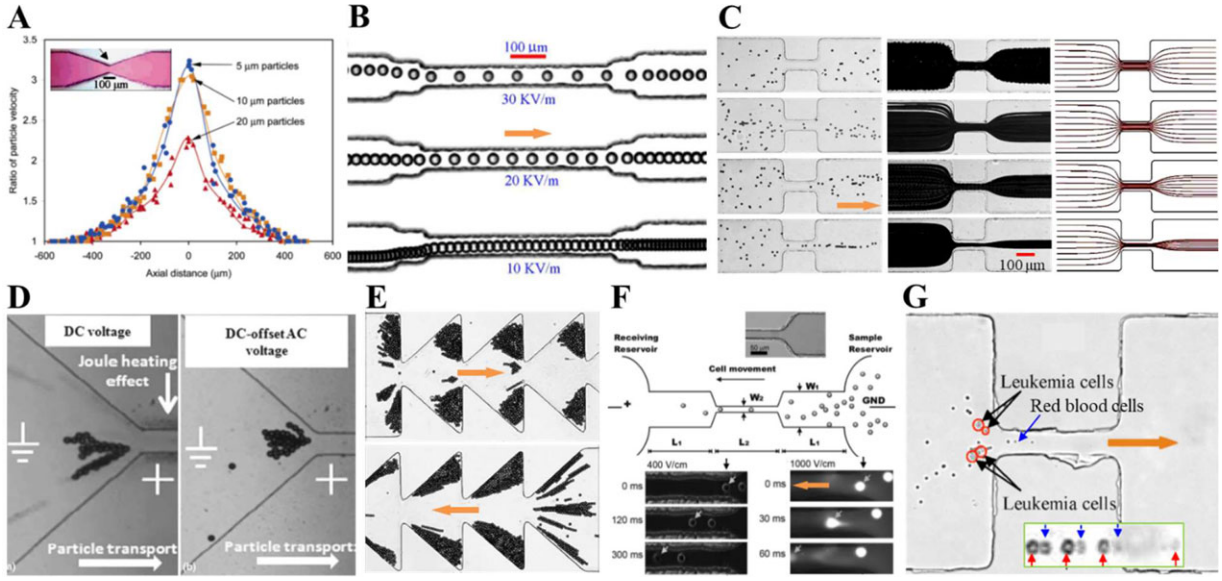

Figure 10. Electrokinetic focusing, trapping, and poration of particles in straight microchannels with insulating hurdles patterned on the sidewalls. (A) DC electrokinetic velocity ratios in between the throat and channel for particles of different sizes traveling along the centerline of a converging-diverging microchannel (see the inset picture). Adapted with permission from Xuan et al. [155], © 2005 American Chemical Society. (B) Superimposed images of 40 μm particles in the electroosmotic flow through a 50 μm wide microchannel constriction under varying DC electric fields. Adapted with permission from Xuan et al. [63], © 2006 Elsevier; (C) Dielectrophoretic focusing of 10 μm particles in a 56 μm wide constriction microchannel under a fixed 100 V/cm electric field with the AC to DC field ratio being varied from 0 to 1, 4, and 9 (top to bottom). Adapted with permission from Zhu and Xuan [42], © 2009 Wiley-VCH. (D) Dielectrophoretic concentration of 15 μm particles in a tapered contraction microchannel under 4250 V/cm DC (left) and 40 V/cm DC-biased 800 V/cm AC electric fields. Adapted with permission from Lewpiriyawong et al. [157], © 2012 Springer. (E) Dielectrophoretic patterning of 10 μm particles in an asymmetric ratchet microchannel when the particles move in different directions. Adapted with permission from Kale et al. [158], © 2014 Institute of Physics. (F) DC electrokinetic poration (lower left) and lysis (lower right) of mammalian cells in a constriction microchannel. Adapted with permission from Wang and Lu [159], © 2006 American Chemical Society. (G) Integrated concentration of leukemia cells and lysis of red blood cells (see the inset) in a constriction microchannel under a 30 V/cm DC-biased 170 V/cm AC electric field. Adapted with permission from Church et al. [161], © 2010 American Institute of Physics.

particles in 10 mM sodium buffer through a 50 μm wide neck of a 125 μm wide straight rectangular microchannel under 100 V/cm DC electric field (Fig. 10B). For particles with small confinement ratios, Zhu and Xuan [42] proposed the use of DC-biased AC electric field for effective particle manipulation in a single microchannel constriction. They demonstrated an efficient electrokinetic focusing of 10 μm particles in 1 mM KCl solution through a 56 μm wide constriction in a straight 310 μm wide microchannel under 10 V/cm DC/90 V/cm AC (Fig. 10C). A similar idea was later employed by Lewpiriyawong et al. [157] to concentrate particles and cells in a tapered contraction microchannel. The authors found

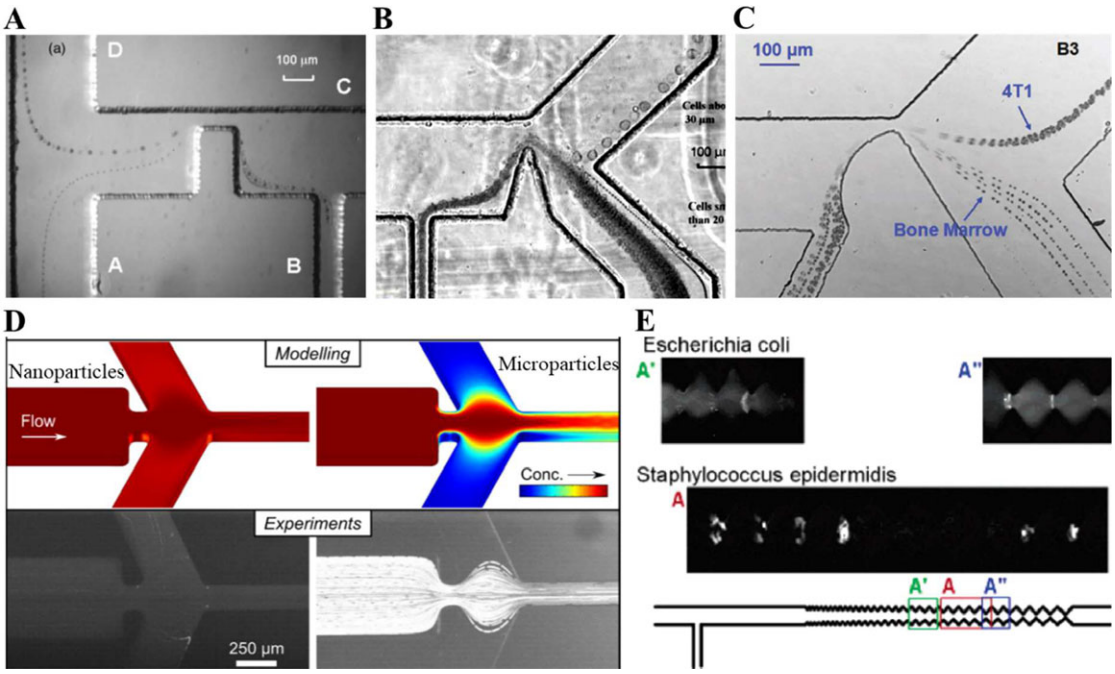

Figure 11. Electrokinetic separation of particles in straight microchannels with insulating hurdles patterned on the sidewalls. (A) Dielectrophoretic separation of 5.7 and 15.7 μm particles in a microchannel with a rectangular hurdle under an average DC electric field of 150 V/cm. Adapted with permission from Kang et al. [162], © 2006 Wiley-VCH. (B) Dielectrophoretic separation of large and small breast cancer cells in a microchannel with a triangular hurdle. Adapted with permission from Kang et al. [163], © 2008 Springer. (C) Dielectrophoretic separation of 4T1 breast cancer cells and bone marrow cells in a microchannel with an arc hurdle. Adapted with permission from Sun et al. [164], © 2012 American Chemical Society. (D) DEP-based separation of 500 nm (left column) and 2.5 μm (right column) particles in a microchannel with a pair of rectangular hurdles under an average DC electric field of 1900 V/cm. Adapted with permission from Abdallah et al. [166], © 2015 American Chemical Society. (E) DEP-based separation of live and dead *E. coli* cells in a sawtooth microchannel with dielectrophoretic field gradients under an average DC electric field of 300 V/cm. Adapted with permission from Pysher and Hayes [167], © 2007 American Chemical Society.

that the strength of the DC-biased AC electric field can be more than 85% smaller than that of the DC electric field for dielectrophoretic trapping of 15 μm particles before the 60 μm wide contraction (Fig. 10D). Further, Kale et al. [158] studied the development of dielectrophoretic trapping of 10 μm particles in a 500 μm wide asymmetric ratchet microchannel. They observed dissimilar trapping patterns within the ratchets (with 100 μm wide throats) when particles move from left to right and from right to left, respectively (Fig. 10E).

In another interesting work, Lu's group [159] developed a simple DC electrokinetic technique to rapidly porate and lyse biological cells in constriction microchannels. The exposure time of cells to the high electric field within the constriction can be controlled by the electrokinetic cell velocity and the length of the constriction. Wang and Lu [159] demonstrated a high throughput electroporation and lysis of Chinese hamster ovary cells in 10 mM phosphate buffer through a 213 μm wide straight rectangular microchannel with a 2-mm long, 33 μm wide constriction in the middle under the DC electric fields of 500 and 1000 V/cm, respectively (Fig. 10F). Wang et al. [160] also demonstrated an efficient lysis of *Escherichia coli* cells in a similar constriction microchannel when the local electric field strength in the constriction reached 1,000–1,500 V/cm. This threshold field strength is considerably lower than the value reported in the literature due possibly to the longer exposure time of cells to the locally high electric field. In a later study, Church et al. [161] demonstrated an integrated electrical concentration of leukemia cells and lysis of red blood cells in PBS solution through a 40 μm wide constriction in a 400 μm wide straight rectangular microchannel. The electrokinetic cell motion can be precisely controlled by adjusting the DC field component, which leads to an easy switch between concentration and lysis of red blood cells at the constriction region (Fig. 10G).

Kang et al. [162] demonstrated a size-based separation of polystyrene particles in a 300 μm wide microchannel with a rectangular hurdle via DC iDEP (Fig. 11A). The particle mixture is prefocused by a particle-free sheath flow and then split into two streams because of the size-sensitive dielectrophoretic force induced at the 30 μm wide constriction [128]. The authors also developed a 2D LTM-based numerical model that considered both the dielectrophoretic motion and the wall-induced lateral migration. The predicted particle trajectories agree reasonably with the experimental images. Kang et al. [163] later extended the same method

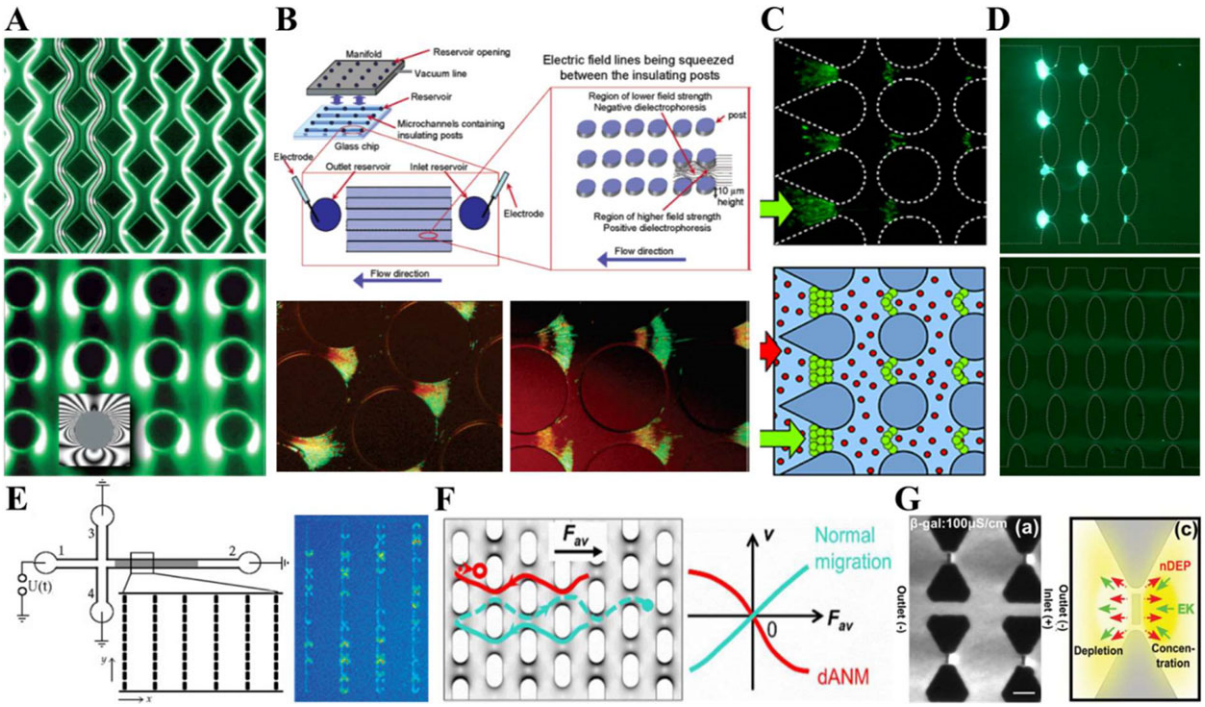

Figure 12. Electrokinetic manipulation of particles in straight microchannels with an array of insulating posts patterned on the bottom walls. (A) Fluorescence images of streaming (top) and trapping (bottom) DEP of 200 nm particles in microchannels patterned with diamond-shaped and circular insulating posts, respectively. Adapted with permission from Cummings and Singh [173], © 2003 American Chemical Society. (B) Simultaneous concentration and separation of live (green) and dead (red) *E. coli* bacteria (bottom) via iDEP in an array of circular insulating posts (top). Adapted with permission from Lapizco-Encinas et al. [175], © 2004 American Chemical Society. (C) Schematic illustrating the enhanced enrichment of cells because of the addition of small filler particles. Adapted with permission from Saucedo-Espinosa and Lapizco-Encinas [184], © 2017 American Chemical Society. (D) Dielectrophoretic trapping of 200 nm particles in equal-length microchannels with 3 (top) and 21 (bottom) columns of elliptical posts. Adapted with permission from Perez-Gonzalez et al. [185], © 2018 American Chemical Society. (E) Dielectrophoretic trapping of fluorescently stained T2 DNA (right) in an array of rectangular insulating posts (left). Adapted with permission from Regtmeier et al. [190], © 2007 American Chemical Society. (F) Separation of μm and sub-μm colloidal particles and organelles in a nonlinear post array under a periodic action of electrokinetic and dielectrophoretic forces. Adapted with permission from Luo et al. [191], © 2016 American Chemical Society. (G) Fluorescence microscopy images for the iDEP concentration (right, schematic) of β-galactosidase (left) at the inlet side of insulating nanoposts. Adapted with permission from Nakano et al. [192], © 2015 Royal Society of Chemistry.

to separate biological cells. In order to reduce the exposure time of cells to high electric field and as well lower the adverse effects of Joule heating, they replaced the rectangular hurdle with a triangular one. They demonstrated in this new device a continuous separation of mammalian cells under a weak DC electric field of less than 50 V/cm (Fig. 11B). Sun et al. [164] further integrated such a DC iDEP cell sorter with a metal-oxide semiconductor field-effect transistor-based microfluidic Coulter counter for a simultaneous on-chip cell separation and sizing. Moreover, they found that an arc hurdle, in place of the triangular hurdle in Fig. 11B, can assist forcing cells to enter into the constriction region at approximately equal positions and hence enhance the separation performance (Fig. 11C).

Ros' group [165] developed a microfluidic device to sort nanoparticles from microparticles in a constriction microchannel using DC iDEP. They later revised the design of their device by altering the deflection angle of the side collection channels, and optimized both the geometrical dimensions and input parameters through a combined experimental and numerical study [166]. The new device is capable of fractionating nanobeads from microbeads with a high sorting efficiency (Fig. 11D) as well as sorting protein crystals into sub-micrometer size fractions for future serial femtosecond crystallography. Hayes' group [167] described a microfluidic device with a sawtooth microchannel that adds a longitudinal gradient feature to the iDEP technique for separation of complex biological particles and structures in a single channel. The production of stronger local field gradients along a global gradient in such a microchannel allows particles to be isolated according to their characteristic physical properties including charge, polarizability, deformability, and so on. Hayes' group have demonstrated the use of such a gradient insulator-based dielectrophoresis technique for the separation of live/dead bacteria cells (Fig. 11E) [167] and blood cells from biomarkers [168] as well as nano to submicron particles [169], and so on. In addition, Mohammadi et al. [170, 171] reported interesting studies on DC electrokinetics-based blood plasma separation in straight microchannels with varying cross sections.

4.3.2 Insulating posts patterned on the bottom walls of microchannels

The concept of iDEP was first proposed and implemented by Cummings and Singh [172]. They identified two regimes of DEP when a sufficiently large DC electric field was applied across an insulating post array [173]. Streaming DEP takes place when DEP dominates diffusion but is overcome by electrokinetic flow, where particles get concentrated in areas of electric field extrema and travel electrokinetically down the array in flowing streams. Trapping DEP occurs if DEP dominates over both diffusion and electrokinetic flow, where particles get immobilized and enriched on the insulating posts (Fig. 12A). Chou et al. [174] developed an electrodeless trap using insulating constrictions at far lower frequencies than what are feasible with metallic trapping structures because of water electrolysis. They demonstrated such electrodeless DEP could be used to concentrate and pattern both single-strand and double-strand DNA. The same group later used diffusive mixing and dielectrophoretic trapping to lyse *E. coli* cells in a microfabricated environment and trap the released chromosome while the other components of the lysate was removed by a DC electrokinetic flow [39]. Lapizco-Encinas et al. [175, 176] later demonstrated the application of DC iDEP for the selective concentration of live and dead bacteria in an array of circular insulating-post structures that were fabricated onto glass (Fig. 12B). Her own group further performed extensive studies to understand and optimize the iDEP device performance [177–181] as well as exploring new applications [182, 183]. For example, Saucedo-Espinosa and Lapizco-Encinas [184] reported an over 100 times dielectrophoretic enrichment of yeast cells under a low DC electric field in the presence of filler particles because of the resulting particle–particle interactions (Fig. 12C). Perez-Gonzalez et al. [185] observed that reducing the number of columns of insulating posts significantly decreases the required voltage to dielectrophoretically trap particles because of the alteration of the electric field distribution within the post array (Fig. 12D).

Ros' group has also made significant contributions to electrokinetic particle manipulation in straight microchannels with an insulating post array [186–189]. For example, Regtmeier et al. [190] demonstrated an efficient and fast dielectrophoretic separation of DNA according to length in periodically arranged rows of rectangular posts (Fig. 12E). This is a result of the length-dependent DNA polarizability that leads to DNA fragment-sensitive thermal escape out of the dielectrophoretic traps in the direction of electrophoretic force. Luo et al. [191] developed a counterintuitive separation mechanism for micro and sub-micron colloidal particles and organelles via particle transport in a nonlinear insulating post array. They revealed that under a periodic action of electrokinetic and dielectrophoretic forces the deterministic migration of larger particle goes against the applied force, that is, of deterministic absolute negative mobility, whereas normal response is obtained for smaller particles (Fig. 12F). Nakano et al. [192] extended the use of DC iDEP to concentrate β-galactosidase proteins at the inlet of nano-constrictions that were created between the tips of triangular microposts to achieve high electric field gradients. Interestingly, they observed a unique voltage dependent β-galactosidase concentration, which was attributed to ion concentration polarization at the nano-constrictions (Fig. 12G). In addition, Davalos and his coworkers contributed to postarray iDEP devices as well [193, 194].

4.4 One-dimensional depthwise in-channel variations

Due to the fabrication complexity, there are much less studies on electrokinetic manipulation of particles in straight microchannels with variations in the depth direction of the cross section. These 2D depthwise constrictions span across the entire channel width and may be straight or coherently curved. Barrett et al. [195] used a two-level isotropic etch of a glass substrate to create 3D ridge-like structures in 50 μm deep microchannels with a 5 μm gap. The dielectrophoretic force that results from the DC electric field gradients near the ridges deflects *Bacillus subtilis* cells parallel to the ridges toward the center channel. It, however, has a negligible impact on 200-nm diameter polystyrene particles under the same conditions (Fig. 13A). Hawkins et al. [40] fabricated using hot embossing a thermoplastic microdevice with an insulative constriction in channel depth, whose angle of incidence with the direction of flow varies continuously across the channel width. They manipulated particles with DC-biased AC electric fields, which generated continuous output streams of particles with a transverse outlet position specified by the particle mobility ratio in Eq. (19). They demonstrated a dielectrophoretic spectrometer that separates particles and controls their transverse channel position (Fig. 13B). Täuber et al. [196] used a two-step contact lithography to fabricate a microchannel with an arc-shaped insulating ridge. They demonstrated for the first time a continuous iDEP separation of linear and covalently closed circular DNA molecules based on conformation. Moreover, they separated in the same device linear DNA fragments with the minimal size difference of 16.7% under DC-biased AC electric fields (Fig. 13C). This resolution is much better than that reported by Viefhues et al. [197] in a similar nanofluidic device. Viefhues [198] also fabricated a microchannel with an asymmetric S-shaped ridge extending over the full channel width. They demonstrated in this microfluidic device reversible mixing and demixing of 20 and 100 nm polystyrene particles via electrodeless DEP at the 620-nm thick constriction (Fig. 13D).

4.5 Two-dimensional in-channel variations

There have also been a few reported studies on electrokinetic manipulation of particles in straight microchannels with variations in both the width and depth directions of the cross section. These 3D constrictions can significantly increase the local electric field gradients for enhanced DEP.

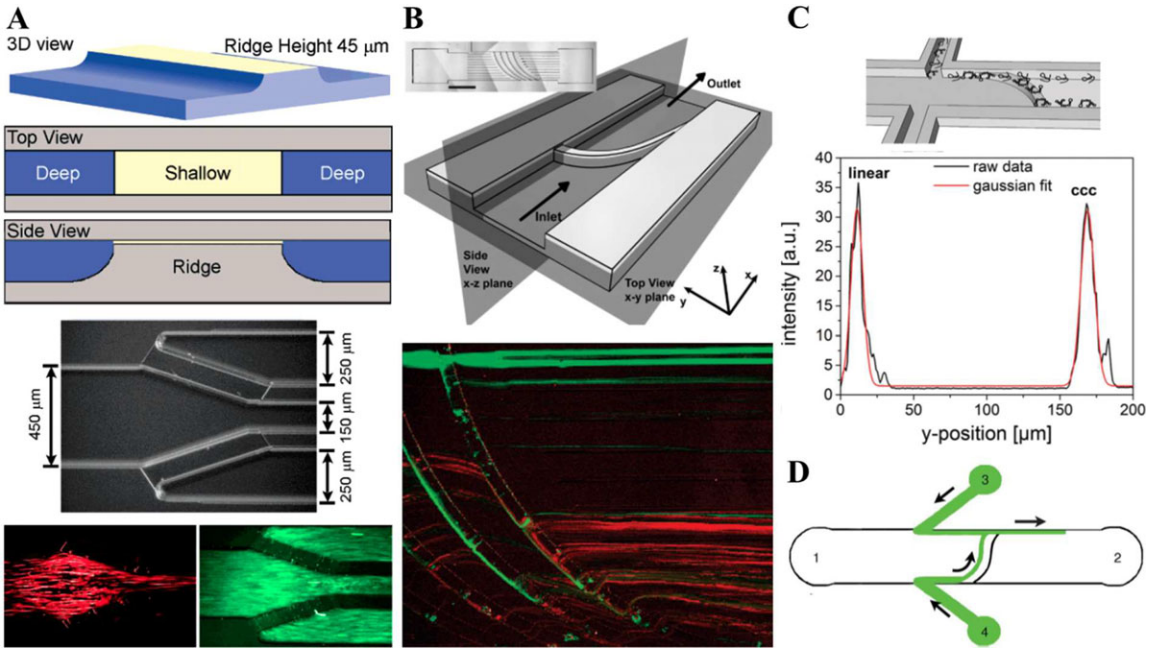

Figure 13. Electrokinetic manipulation of particles in straight microchannels with a 2D depthwise constriction. (A) Schematic representations of an insulative ridge (upper panel); Micrograph of a manufactured device that has two ridges in a microchannel with one inlet and three outlets (middle panel); Experimental images show the particle-specific confinement using iDEP under a 300 V/cm DC electric field, where *B. subtilis* cells (red) flow down only the center channel while 200 nm diameter particles (green) flow freely through all three outlet channels (lower panel). Adapted with permission from Barrett et al. [195], © 2005 American Chemical Society. (B) Schematic of a channel geometry with a curved insulative ridge (upper panel); Pseudo color time lapse for the separation of 2 μm (green) and 3 μm (red) particles in such a channel with a constriction ratio of 10 under a 50 V/cm DC/ 750 V/cm AC electric field (lower panel). Adapted with permission from Hawkins et al. [40], © 2007 American Chemical Society. (C) Fluorescence intensity plot (lower panel) of a continuous-flow separation of linear and covalently closed circular (ccc) DNA in a microchannel with a curved ridge (upper panel) under a DC-biased AC (12.4 kV/cm at the 670 nm deep constriction) electric field. Adapted with permission from Täuber et al. [196], © 2017 Royal Society of Chemistry. (D) Sketch of a microchannel with an S-shaped ridge (620 nm deep constriction) for the mixing of 20 nm and 100 nm nanoparticles (injected through channels 3 and 4, respectively) under a DC-biased AC electric field. Adapted with permission from Viefhues [198], © 2012 Royal Society of Chemistry.

As a result, the required electric field magnitude for particle manipulation can be substantially decreased, which reduces both the electrical and thermal damages on samples and devices [199, 200]. Braff et al. [201] used micro-milling to fabricate devices with 3D features that exhibit very large constriction ratios. They used their 3D iDEP (3DiDEP) device to trap particles at average DC electric fields one order of magnitude smaller than 2D designs with the same footprint (Fig. 14A). The authors [202] later used their device for a strain-level discrimination of bacterial cells based on their surface properties. Nakidde et al. [203] developed a 3D passivated-electrode, iDEP (3D πDEP) microchip, which integrates the benefits of eDEP and 3DiDEP with the goal of improving particle trapping efficiency at low voltages with a wide frequency range (Fig. 14B). Their chip was fabricated by making 3D structures in silicon using reactive ion etching [204]. Liao and Chou [205] reported a molecular dam to enhance protein enrichment in nanofluidic channels by 3DiDEP in physiological buffers under DC-biased AC electric fields. They used dielectric nanoconstrictions down to 30 nm to magnify the applied electric field by 105-fold when combined with a micro- to nanofluidic step interface (Fig. 14C). In an earlier study, Liao et al. [206] found that the addition of a critical DC field offset to the nDEP trapping could result in an elliptical-shaped protein depletion zone that extends along the device axis causing a rapid protein preconcentration along the constriction sidewall direction. They explained the observation using the balance of electrokinetic forces (Fig. 14D). Li et al. [207] reported a similar microchip with microchannels and nano-slits in between for DEP trapping of DNA molecules in both high and low conductive media under DC electric fields (Fig. 14E).

4.6 Tunable in-channel variations

There are a couple of studies on the electrokinetic manipulation of particles in straight microchannels with tunable variations in the cross section. These essentially 3D constrictions are formed by oil droplets that can be retreated or advanced. Barbulovic-Nad et al. [208] developed a microfluidic device for particle separation by using an oil droplet to act as an insulating hurdle for DC iDEP. Since the size of the droplet can be changed on the fly, the resulting electric field gradients and in turn particle DEP become adjustable to accommodate varying particle parameters. The authors used the device to

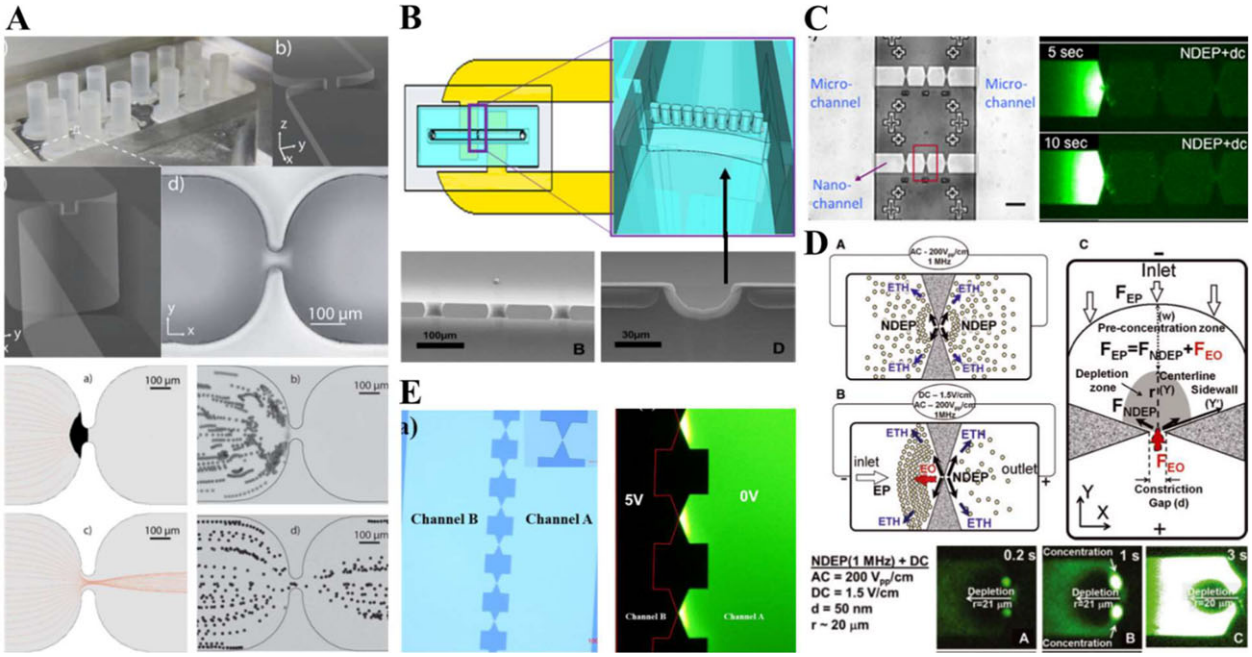

Figure 14. Electrokinetic manipulation of particles in straight microchannels with 3D constrictions in both the width and depth directions. (A) PMMA microfluidic chip with 3D or 2D iDEP microchannels (upper panel); Predicted (left) and experimentally observed (right) motion of 10 μm particles in 3D and 2D iDEP microchannels under the DC electric fields of 10 and 50 V/cm, respectively (lower panel). Adapted with permission from Braff et al. [201], © 2012 Royal Society of Chemistry. (B) Top view schematic of reusable electrodes and 3D insulating features of 3D πDEP microfluidic device (upper panel); SEM images of a fabricated 3D πDEP device from the top (left) and (right) cross section views (lower panel). Adapted with permission from Nakidde et al. [203], © 2015 American Institute of Physics. (C) Optical micrograph of long nanofluidic channels that are connected by microfluidic channels and each seeded with three nano constrictions (left panel); nDEP trapping and damming of proteins under 214 V/cm AC field with a 1.5 V/cm DC bias (right panel). Adapted with permission from Liao and Chou [205], © 2012 American Chemical Society. (D) Schematics of protein preconcentration through a balance of electrokinetic forces (upper panel); Fluorescence images of 50 nm constriction devices showing the formation and development of the depletion zone (lower panel). Adapted with permission from Liao et al. [206], © 2012 Wiley-VCH. (E) Optical image of nano-slits in between two microchannels (left panel); DC dielectrophoretic trapping of DNA near the nano-slits (right panel). Adapted with permission from Li et al. [207], © 2015 American Institute of Physics.

demonstrate a continuous flow separation of 5.7 and 15.7 μm particles under a DC electric field lower than 100 V cm (Fig. 15A). Thwar et al. [209] generated dielectrophoretic potential wells using pairs of insulating oil menisci to shape the DC electric field. The oil menisci are arranged in a configuration similar to the quadrupolar electrodes in eDEP microdevices to produce electric field gradients. The one-pair well produces a focusing effect on particles while the two-pair well results in spatial particle traps. They demonstrated an enhanced trapping and concentration of 10 μm polystyrene particles by increasing the penetration of one of the menisci into the main flow channel (Fig. 15B), which decreased the gap between the menisci and hence reshaped the local electric field.

5 Curved microchannels

5.1 Theoretical analysis

In a curved microchannel, electric field attains the maximum and minimum strengths near the inner and outer walls, respectively, because of the variation in path length for electric current. This is illustrated in Fig. 16A by the electric field contour in an arc microchannel of angle θ (in radians), which induces a dielectrophoretic force acting on a particle that travels through the arc channel following the electric field lines at the velocity, $\mathbf{U}_{EK}$. The resulting dielectrophoretic motion, $\mathbf{U}_{DEP}$, directs the particle radially outward (if nDEP) or inward (if pDEP), which, for prolate spheroidal particles ($b = c$), can be written as [48]:

$$\mathbf{U}_{DEP} = 2(1 + r^2)\mu_{DEP}\frac{\mathbf{E}_{DC}^2}{\Re}\hat{\mathbf{n}}, \tag{20}$$

$$\mu_{DEP} = \frac{a_p^2\varepsilon}{9\eta K_i}\frac{\sigma_p - \sigma}{\sigma + (\sigma_p - \sigma)L_i}, \tag{21}$$

where $\Re$ is the radius of curvature of the local electric field line (Fig. 16A) that depends on the radius of the arc as well as the particle position, a_p is the equivalent spherical radius of the spheroid, $K_i \geq 1$ is the correction factor for the particle shape-dependence of the Stokes' drag that decreases to 1 for spheres [47, 210], and $L_i \leq 1/3$ is the depolarization factor that becomes 1/3 for spheres [48, 210]. The competition of

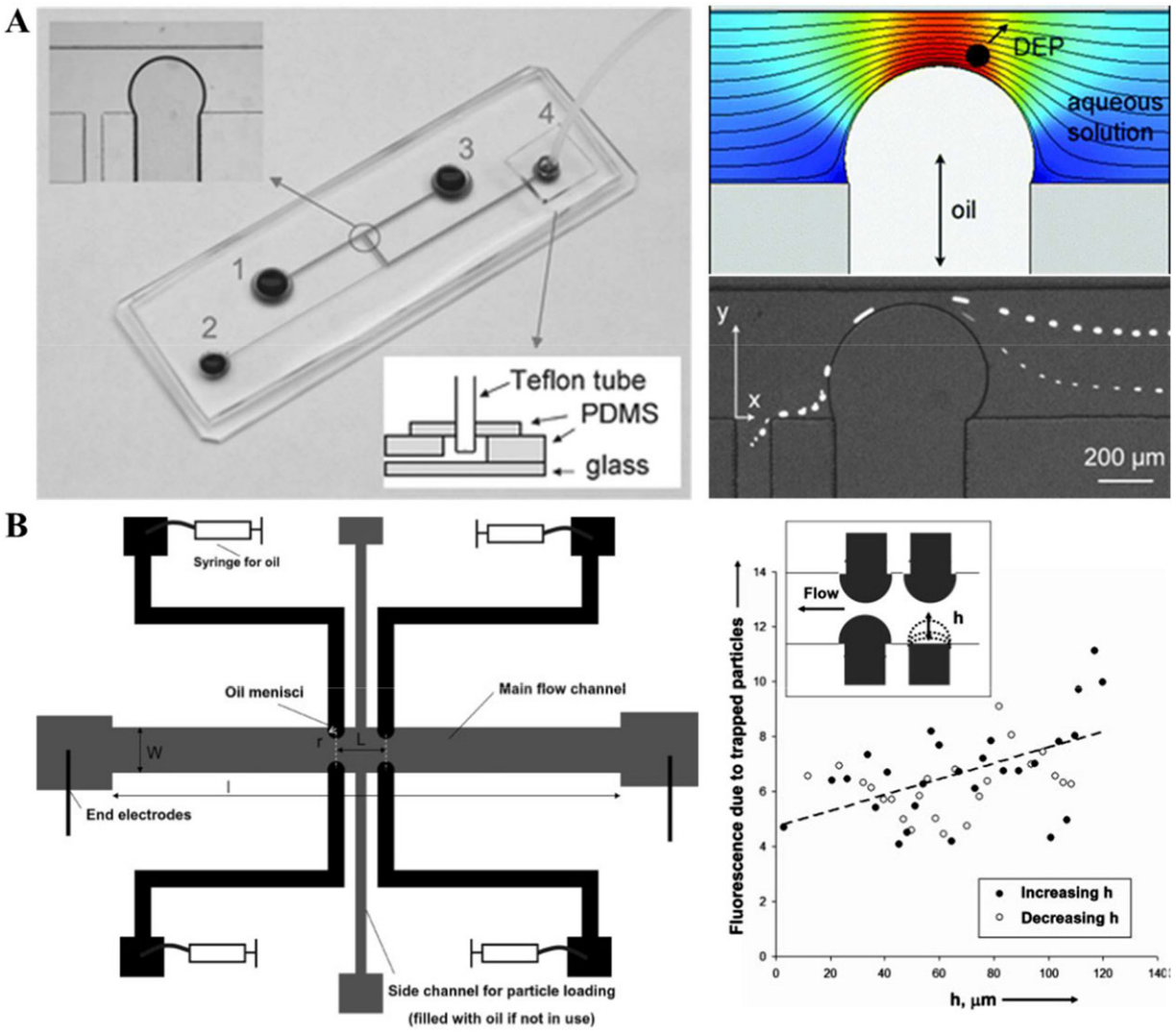

Figure 15. Electrokinetic manipulation of particles in straight microchannels with tunable constrictions formed by droplets. (A) Isometric picture of the microfluidic chip, where the oil from branch 4 forms a droplet in the main channel (left panel); Particles are deflected by nDEP across the electric field lines because of the electric field gradients induced by the oil droplet (upper right panel); Observed separation of prefocused 5.7 and 15.7 μm particles after the droplet (lower right panel). Adapted with permission from Barbulovic-Nad et al. [208], © 2006 Royal Society of Chemistry. (B) Schematic of the PDMS-glass device for forming two-pair dielectrophoretic potential wells via a DC electric field across the main microchannel (left panel); Change in fluorescence intensity of 10 μm particles trapped at the center of the gap between the four insulating oil menisci in response to increasing and decreasing the extent of penetration (h) of one of the menisci into the main flow channel (right panel). Adapted with permission from Thwar et al. [209], © 2007 Wiley-VCH.

$\mathbf{U}_{DEP}$ and $\mathbf{U}_{EK}$ results in a cross-stream particle $deflection$ in the arc microchannel:

$$deflection = \frac{U_{DEP}\Re\theta}{U_{EK}} = 2(1+r^2)\theta\, E_{DC}\frac{\mu_{DEP}}{\mu_{EK}}, \tag{22}$$

which can be significantly increased by the use of a serpentine or a spiral that consists of multiple half or full loops (note one full loop has a rotating angle of 2π) while still having a compact footprint. It is, however, important to note the particle $deflection$ in Eq. (22) is independent of the radius of the curvature (or simply the arc) even though the dielectrophoretic velocity in Eq. (20) does increase in a smaller radius arc. This is because the traveling distance decreases in a smaller radius arc and hence the exposure time of particles to curvature-induced dielectrophoresis (C-iDEP) also reduces. In addition, similar to the analysis in Section 4.1, the particle $deflection$ in an arc microchannel is associated with the electrokinetic to dielectrophoretic mobility ratio, which for spheroidal particles is rewritten as:

$$\frac{\mu_{EK}}{\mu_{DEP}} = \frac{9(\zeta_p-\zeta_w)K_i}{a_p^2}\frac{\sigma+(\sigma_p-\sigma)L_i}{\sigma_p-\sigma}. \tag{23}$$

Note that Eq. (23) is reduced to Eq. (19) for spherical particles with $K_i = 1$ and $L_i = 1/3$. As their mobility ratio is a function of particle size (a_p), surface charge (ζ_p), conductivity (σ_p), and shape (K_i and L_i), particles can be

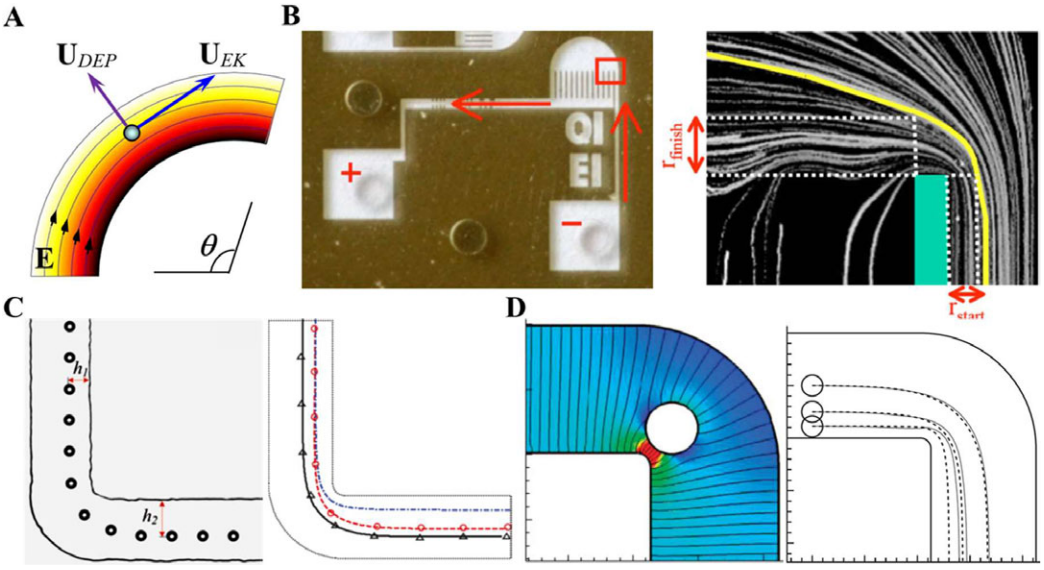

Figure 16. (A) Illustration of C-iDEP experienced by a particle moving electrokinetically through an arc microchannel. (B) A photograph of the microfluidic channel, where the red arrows indicate the flow direction and the red rectangle shows the region of observation (left panel); Top-view image showing the trajectories of DNA molecules flowing around the 90° sharp corner in the region of observation (right panel). Adapted with permission from Parikesit et al. [214], © 2008 American Institute of Physics. (C) Trajectories of a 10 μm diameter particle travelling through an L-shaped rectangular microchannel under a 120 V/cm DC electric field (left panel); Comparison between experimental (symbols) and predicted (lines) particle trajectories (right panel). Adapted with permission from Ai et al. [215], © 2010 American Chemical Society. (D) Equipotential contours plotted over the electric field strength around a particle moving through a bent cylindrical pore (left panel); The effect of initial position on particle trajectories where the solid lines represent the predictions from the boundary-element method and the dashed lines represent the results from the point-dipole method (right panel). Adapted with permission from House and Luo [216], © 2011 Wiley-VCH.

dielectrophoretically deflected to different flow paths in a curved microchannel and hence be separated based on one or more of the intrinsic properties. This technique is termed as curvature-induced DEP or C-iDEP in short by the author's group [211].

5.2 Microchannels with a single bend

The electrophoretic motion of a spherical particle through a 90° corner (as part of a T-junction) was first studied by Ye and Li [212], who considered in a 2D numerical model the hydrodynamic force while ignoring the electric force acting on the particle. A similar approach was later employed by Davison and Sharp [213] to study the electrophoretic motion of a cylindrical particle through a 90° turn. Due to the small Reynolds number of electroosmotic flows, particles experience no net cross-stream migration in the absence of the electric force. Parikesit et al. [214] observed that C-iDEP around a sharp corner can actually cause size-dependent trajectories of DNA macromolecules in a microfluidic channel of 0.4 μm depth (Fig. 16B). Their numerical simulation of the electrokinetic force distribution inside the microchannel was found to agree qualitatively with the experimentally observed trajectories. They envision that the observed DNA migration may be potentially used to sort DNA molecules by size at low DC electric fields. Ai et al. [215] presented a combined numerical and experimental study of the electrokinetic transport of spherical polystyrene particles through an L-shaped microchannel under DC electric fields. They considered both the hydrodynamic and electric forces on the particle by integrating the hydrodynamic and Maxwell stress tensors over the particle surface directly. Their predictions of the DEP-induced particle trajectory shift are in quantitative agreement with the experimental observation (Fig. 16C). House and Luo [216] applied a numerical approach based on the boundary-element method to solve the coupled electric field, fluid flow, and particle motion in particle electrophoresis through a bent cylindrical pore. Their method can handle much closer particle–wall distances than the other numerical approaches such as the finite element method. The authors found that as a nonconducting particle comes close to a nonconducting wall, its finite size has an increasingly important effect on its own transient motion (Fig. 16D). A similar approach was also employed by Cetin et al. [217] to model the dielectrophoretic particle motion in a constriction microchannel.

5.3 Serpentine microchannels

Figure 17A shows a schematic analysis of the particle motion in the electroosmotic flow through one period of a serpentine microchannel, where the background displays the electric field contour and lines. Since the inner and outer corners switch between the left and right turns of the serpentine,

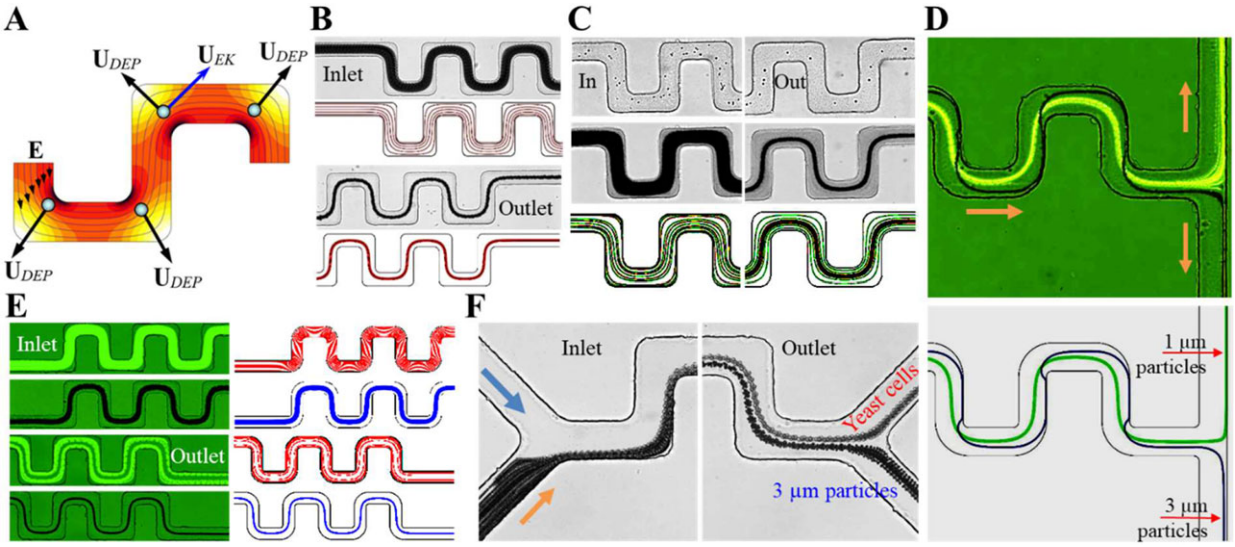

Figure 17. Electrokinetic manipulation of particles in serpentine microchannels. (A) Schematic illustrating the mechanism of particle focusing via C-iDEP in a serpentine microchannel. (B) Experimental and numerical demonstration of C-iDEP focusing of 10 μm particles at the inlet and outlet of a 50 μm wide serpentine microchannel under a 100 V/cm DC electric field. Adapted with permission from Zhu et al. [218], © 2009 Springer. (C) Experimental and numerical results of C-iDEP focusing and filtration of yeast cells from *E. coli* bacteria in a serpentine microchannel under a 100 V/cm total electric field with a AC to DC ratio of 2. Adapted with permission from Church et al. [219], © 2009 American Institute of Physics. (D) Continuous separation of 3 μm (plain) and 1 μm (fluorescent) particles at the exiting bifurcation of a serpentine microchannel under a total electrical field of 880 V/cm with a AC to DC ratio of 15. Adapted with permission from Church et al. [220], © 2011 Wiley-VCH. (E) Experimental and numerical images showing the sheathless C-iDEP separation of 2.2 μm (fluorescent, pDEP) and 5 μm (plain, nDEP) particles in a serpentine microchannel under a 200 V/cm DC-biased AC electric field. Adapted with permission from Church et al. [221], © 2010 Institute of Physics. (F) Superimposed images showing the sheath-flow separation of yeast cells and 3 μm polystyrene particles at the inlet and outlet bifurcations of a serpentine microchannel via C-iDEP under a 100 V/cm DC electric field. Adapted with permission from Zhu et al. [222], © 2011 Springer.

particles will experience a dielectrophoretic motion of alternate directions. For the case of nDEP, particles tend to be deflected toward the channel center region at each turn (Fig. 17A), leading to a focused particle stream along the channel centerline. This analysis was first verified experimentally and numerically by Zhu et al. [218], who studied the C-iDEP focusing of 5 and 10 μm diameter polystyrene particles in a 50 μm wide serpentine microchannel with sharp-angle turns. They demonstrated an efficient focusing of those microparticles within a 1 cm-long serpentine section under a DC electric field on the order of 100 V/cm (Fig. 17B). Increasing the field magnitude and/or parallelizing the microchannel can significantly increase the flow throughput. Church et al. [219] later extended this C-iDEP technique to focus biological cells in a serpentine microchannel using DC-biased AC electric fields. They also demonstrated a continuous electrokinetic focusing and filtration of yeast cells from smaller *E. coli* cells in the serpentine microchannel, for which the experimental observations agree reasonably with the predicted cell trajectories (Fig. 17C).

Church et al. [220] also found that depending on the magnitude of the turn-induced dielectrophoretic force, particles travelling electrophoretically through a serpentine microchannel may migrate toward the centerline or bounce between the two sidewalls. They utilized these distinctive focusing and bouncing phenomena to implement a C-iDEP separation of 1 and 3 μm polystyrene particles under a DC-biased AC electric field with a total strength of 880 V/cm within the serpentine section (Fig. 17D). In another study, Church et al. [221] demonstrated the centerline and sidewall focusing of the same particles in a serpentine microchannel via negative and positive C-iDEP, respectively, which was implemented by changing only the electric conductivity of the suspending fluid. Moreover, they combined these negative and positive dielectrophoretic focusing phenomena to achieve a continuous sheath-free separation of particles by size in a serpentine microchannel under a 200 V/cm DC-biased AC electric field (Fig. 17E). Zhu et al. [222] used the particle size-dependent C-iDEP to separate a prefocused particle mixture in a serpentine microchannel. They further demonstrated a continuous electrokinetic separation of yeast cells (with diameter ranging from 4 to 8 μm) and 3 μm polystyrene particles under a 100 V/cm DC electric field (Fig. 17F).

5.4 Spiral microchannels

Zhang et al. [223] proposed the original idea of using the dielectrophoretic motion induced in a circular microchannel to separate particles with different dielectrophoretic responses. Specifically, the particles with nDEP response are pushed away from the center while those with pDEP response are pulled toward the center. As a result, the nDEP particles end up further from the center than the initial

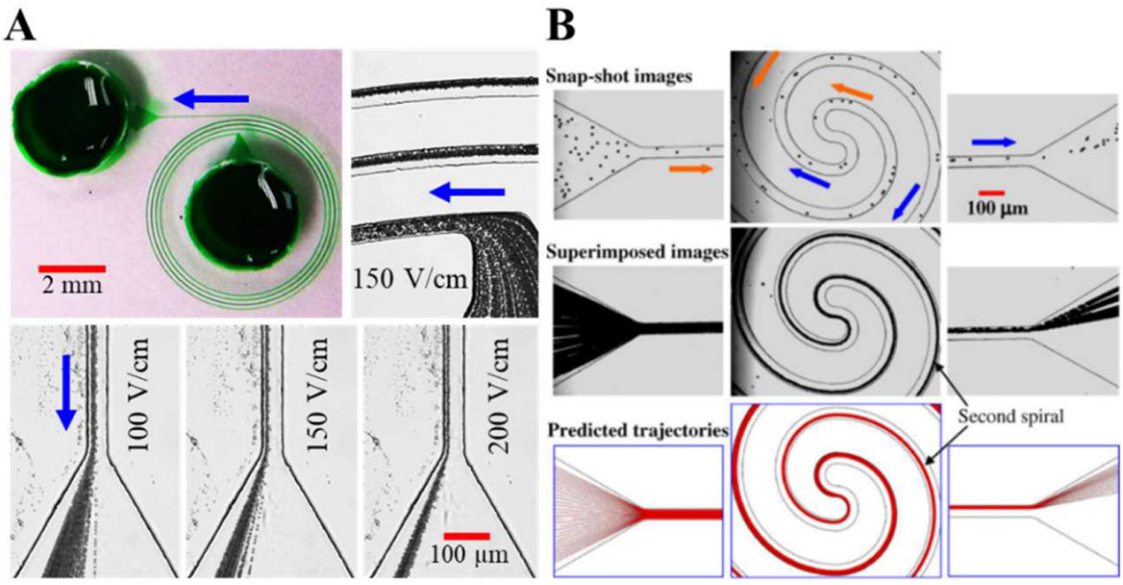

Figure 18. Electrokinetic deflection and focusing of particles in spiral microchannels. (A) Experimental demonstration of C-iDEP focusing of 10 µm particles (lower panel) in a four-loop 50µm wide single-spiral microchannel under varying DC electric fields (upper panel). Adapted with permission from Zhu et al. [224], © 2009 ASME. (B) Experimental and numerical images of C-iDEP focusing of 10 µm particles at the inlet (left), center (middle), and outlet (right) of a 50 µm wide symmetric double-spiral microchannel under a 200 V/cm DC electric field. Adapted with permission from Zhu and Xuan [225], © 2009 Elsevier.

injection point while the pDEP ones end up closer to the center than the initial injection point. For particles with the same dielectrophoretic polarity, the larger particles move toward the outer or inner sidewall of the microchannel at a greater dielectrophoretic mobility. Therefore, the circular channel can be utilized to separate particles of different DEP polarities or sizes in an electroosmotic flow if they are prefocused to the same initial injection position. Zhu et al. [224] studied the dielectrophoretic deflection and focusing of 10 µm particles in a four-loop 50 µm wide single-spiral microchannel (Fig. 18A). Particles were observed to move away from the inner sidewall of each loop in the electroosmotic flow of 1 mM phosphate buffer solution, and eventually reach a near-wall position in a tighter stream at the outlet of the spiral. This C-iDEP focusing increases with the DC electric field strength. Moreover, the equilibrium particle position appears to get slightly closer to the channel wall under a higher electric field. Considering the reservoir inside the single-spiral limits the channel length, Zhu and Xuan [225] later proposed to use a double-spiral microchannel for electrokinetic particle focusing (Fig. 18B). They found that the randomly distributed particles at the inlet of the first spiral are pushed toward the outer wall by C-iDEP, forming a tight stream at the channel center. When the particles travel into the second spiral, they are still subject to C-iDEP but in the opposite direction, due to the switching of the inner and outer walls between the two spirals at the channel center. Eventually, particles move out of the symmetric double-spiral microchannel in a focused stream near the outer wall of the second spiral.

DuBose et al. [226] demonstrated a sheath-free electrokinetic separation of particles in a single-spiral microchannel (Fig. 19A). Their method relies on C-iDEP to focus particles to a tight stream and simultaneously the wall-induced electrical lift to manipulate the aligned particles to size-dependent equilibrium positions. The authors also developed an analytical model to understand the size-based binary and ternary particle separations, which closely predicts the measured particle center–wall distance and the electric field for a complete particle focusing in the spiral. Zhu et al. [227] developed a sheath-free electrokinetic particle separation technique in asymmetric double-spiral microchannels, whose working mechanism is schematically presented in Fig. 19B. Briefly, particles are focused by C-iDEP to a tight stream flowing near the outer wall of the first spiral. In the second spiral, where the electric field magnitude and gradients both get smaller than in the first spiral because of the increased channel width, the aligned particles of dissimilar mobility ratios are deflected away from the inner wall at different rates and hence displaced toward different flow paths. An experimental demonstration of such a C-iDEP separation is presented in Fig. 19C, where a mixture of 5 µm and 10 µm diameter spherical particles is separated at the exiting bifurcation of an asymmetric double-spiral microchannel in 1mM phosphate buffer. The average DC electric fields in the 50 µm wide first spiral is about 180 V/cm. Zhu and Xuan [228] later demonstrated a C-iDEP separation of 10 µm carboxyl-coated and noncoated spherical particles by charge in a microchannel, where the width of the second spiral gradually increases until twice of that of the first spiral. They further separated these two particles along with 5 µm noncoated particles in the same microchannel. They also developed a numerical model to simulate the particle separation processes at varying situations (Fig. 19D). DuBose

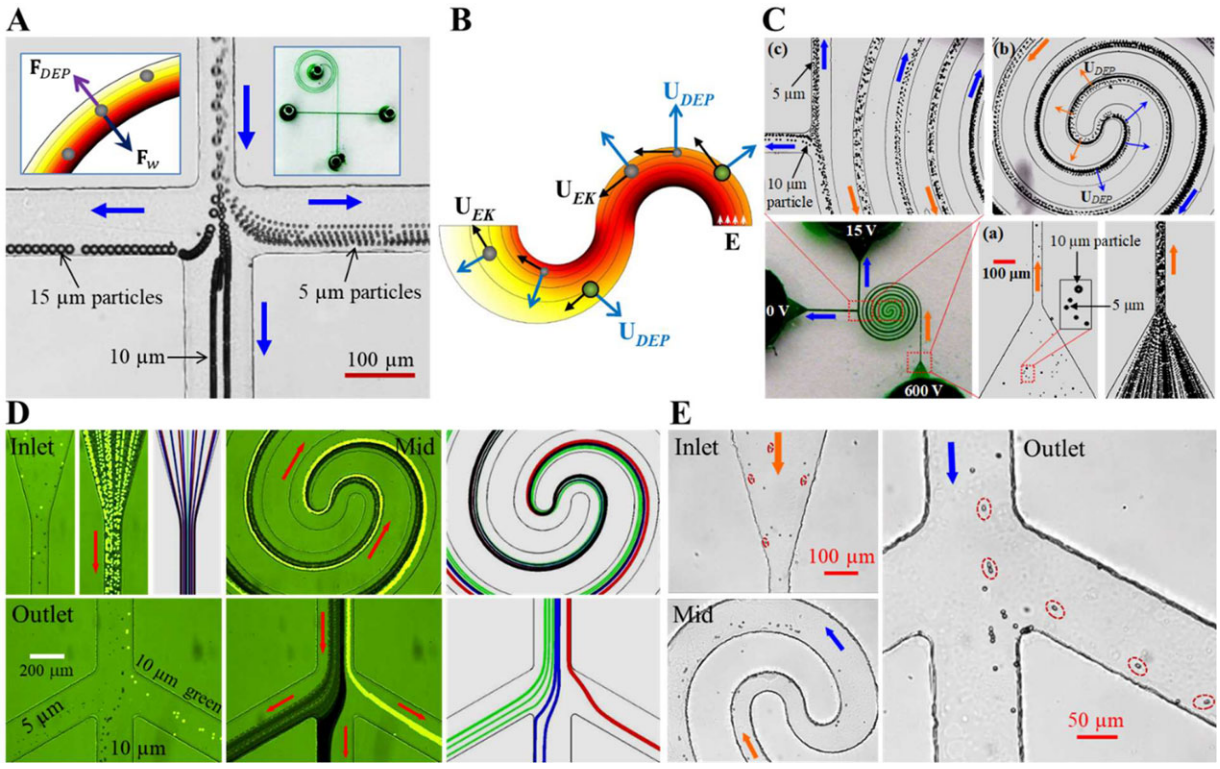

Figure 19. Electrokinetic separation of particles in spiral microchannels. (A) Superimposed image showing a ternary separation of 5, 10, and 15 μm particles in a three-loop 50 μm-wide single-spiral microchannel (see the upper-right inset) via the competition of C-iDEP and wall-induced electrical lift (see the upper-left inset). Adapted with permission from DuBose et al. [226], © 2014 Institute of Physics. (B) Illustration of the mechanism of sheath-free particle focusing and separation via C-iDEP in an asymmetric double-spiral microchannel. Adapted with permission from Zhu and Xuan [228], © 2011 American Institute of Physics. (C) Experimental demonstration of C-iDEP separation of 5 and 10 mm particles at the inlet, center, and outlet of an asymmetric double-spiral microchannel under a DC electric field on the order of 100 V/cm. Adapted with permission from Zhu et al. [227], © 2010 Wiley-VCH. (D) Experimental and numerical demonstration of ternary C-iDEP separation of plain noncoated 5 μm, plain noncoated 10 μm, and fluorescent carboxyl-coated 10 μm particles by size and charge in an asymmetric double-spiral microchannel. Adapted with permission from Zhu and Xuan [228], © 2011 American Institute of Physics. (E) Snapshot images illustrating the shape-based C-iDEP sorting of 5 μm diameter spherical particles and 3.5 μm diameter/6 μm length peanut-shaped particles in an asymmetric double-spiral microchannel under an average 250 V/cm DC electric field. Adapted with permission from DuBose et al. [229], © 2014 American Institute of Physics.

et al. [229] utilized the shape-dependent C-iDEP to separate spherical and peanut-shaped particles of similar volumes in an asymmetric double-spiral microchannel (Fig. 19E).

5.5 Complex microchannels

There are a couple of other studies on the electrokinetic manipulation of particles in microchannels with complex geometries. Chen and Du [230] developed a microfluidic device for rapid and efficient concentration of micro/nanoparticles using DC iDEP in a continuous fluid flow. The microfluidic concentrator is composed of a series of microchannels that are connected through multiple round turns. It converges electric current arithmetically in the flow direction to provide very high field electric field strength and gradient (Fig. 20A, upper panel). In such a concentrator, streaming and trapping DEP of particles take place simultaneously. Multiple trapping regions can be formed and the location of particle trapping depends on the strength of the applied electric field. The performance of this particle concentrator was demonstrated by effectively concentrating fluorescent submicron particles. The particle trapping zone was observed to expand further downstream with the increase of DC electric field (Fig. 20A, lower panel), which agrees with the distribution of the predicted electric field and DEP force. Li et al. [231] presented a DEP-based microfluidic device that incorporates round hurdles within an S-shaped microchannel for continuous particle manipulation and separation. Local nonuniform electric fields are generated by the combination of obstacles (see Section 4.1) and curvature (see Section 5.1), which induce nDEP of particles travelling electrokinetically through the microchannel (Fig. 20B, upper panel). The authors demonstrated in this device a size-based separation of 10 μm and 15 μm polystyrene particles under an average DC electric field of 130 V/cm. The whole process of particle motion in the microchannel is reasonably simulated by a COMSOL® model (Fig. 20B, lower panel).

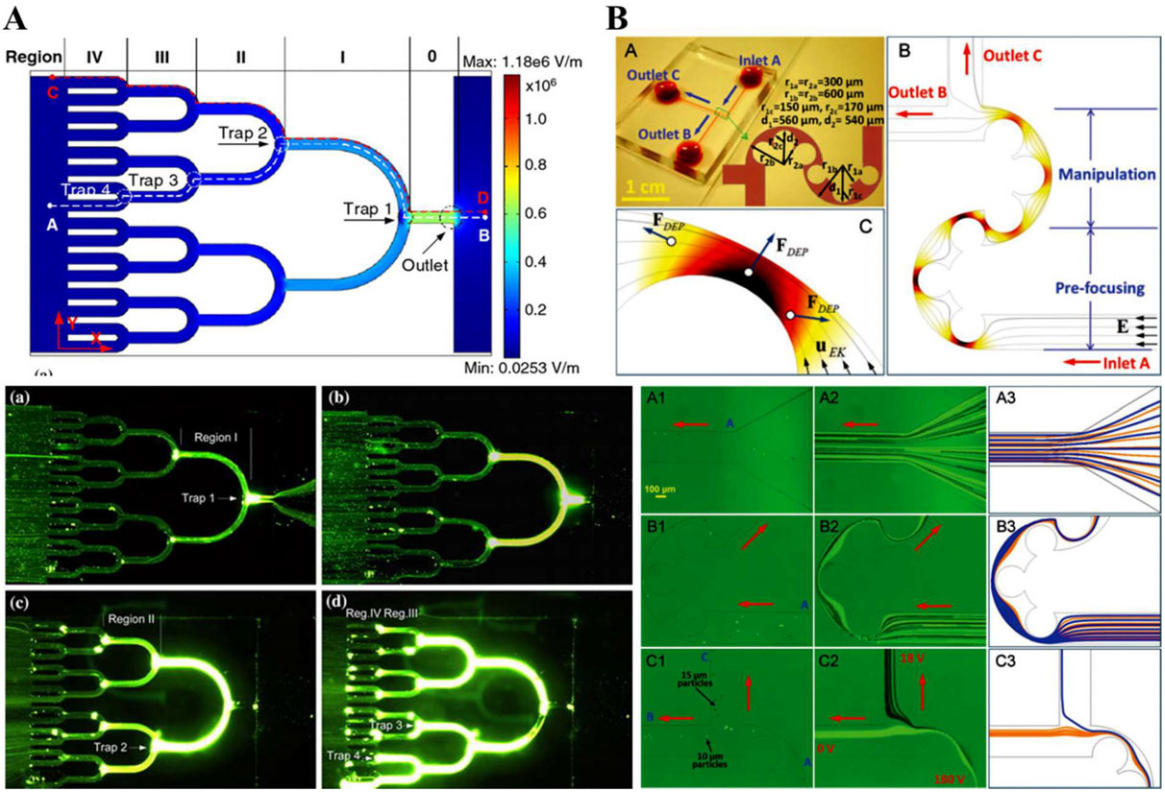

Figure 20. Electrophoretic manipulation of particles in microchannels of complex geometries. (A) Electric field distribution in a particle concentrator composed of a series of microchannels, where four trapping regions, I–IV, are indicated on the plot (upper panel); Enrichment of submicron fluorescent polystyrene particles in the microfluidic concentrator, where the particle trapping zone expands from Region I to Region IV under increasing DC voltages from 300 to 600 V (lower panel). Adapted with permission from Chen and Du [230], © 2010 Springer. (B) Photograph of an S-shaped microchannel embedded with multiple round hurdles along with the illustration of electric field (contours and lines) and DEP for particle manipulation (upper panel); Experimental and numerical demonstration of a continuous separation of 10 and 15 μm particles in the microchannel under an average DC electric field of 130 V/cm. Adapted with permission from Li et al. [231], © 2013 Wiley-VCH.

6 Conclusions and perspectives

The DC and DC-biased AC electrokinetic transport of particles have been reviewed in both straight microchannels with uniform or varying cross sections and curved microchannels. The primary attention of this review has been paid to the various electrokinetic particle manipulations (including focusing, trapping, and sorting) via the cross-stream nonlinear electrokinetic motions caused by the wall-induced electrical lift and/or the insulating structure-induced dielectrophoretic force. A summary of these diverse electrokinetic particle manipulations (experiments only) is presented in Table 2. One can see from this table that the current demonstrations of DC or DC-biased AC electrokinetic manipulations have been very limited for nanoparticles because of the strong size dependence of the involved electrical forces (see, e.g., [31] and [90] along with the papers cited therein). Very high electric fields (even just locally) are often necessary in these demonstrations [31, 90]. It is therefore fundamentally interesting and practically useful to understand if any other nonlinear effects may evolve under such harsh conditions such as the reported ultrafast electrophoresis [232] and the modified Helmholtz–Smoluchowski slip velocity [233]. There are a few other research directions in the field that the author considers worthy of future intensive studies and are each explained below:

(1) Current studies on electrokinetic transport and manipulation of particles in microchannels have been focused mainly upon Newtonian fluids despite the fact that many of the chemical and biological fluids in microfluidic applications possess non-Newtonian characteristics [234, 235]. There has been a growing interest in the understanding of fluid rheological effects (e.g., elasticity and shear thinning) on particle motion in both DC electroosmotic [236] and pressure-driven [237–240] flows of non-Newtonian fluids in microchannels. However, the majority of the studies on electrokinetic particle motion are purely theoretical [236], and experimental investigations are desperately lacking. Recent experiments from the author's group [241–243] have reported some astonishing results (with respect to those in Newtonian fluids), such as the oscillation of particle electrophoresis in the DC electroosmotic flow of viscoelastic fluids through a constriction

Table 2. Summary of DC electrokinetic manipulations of particles (experiments only)

Microchannel	Structure	Particles	Manipulation	Electric field (V/cm)		Refs.
				DC	AC	
Straight microchannels with uniform cross sections	Rectangular cross section	5/10 μm PS	2D focusing	100–500	–	[139]
		5/10 μm PS	3D focusing	100–500	–	[140]
		3/5/10 μm PS	2D focusing	100–500	–	[141]
		5/10 μm PS	2D focusing	100–500	–	[143]
	T-shaped	3/5/10 μm PS	Separation	~500	–	[144]
	Bifurcating	5/10/15 μm PS	Separation	~500	–	[145]
	ψ-Shaped	5 μm PS, yeast cells	Separation by charge	~180	–	[146]
	X-shaped	50 μm Janus/oil droplets	Separation by charge	280	–	[147]
Straight microchannels with varying cross sections	rDEP	1/3 μm PS	Focusing/trapping/separation	50	Up to 950	[149]
		3 μm PS	Separation by charge	40	640	[152]
		Live/dead yeasts	Separation by viability	12	140	[153]
	1D widthwise constriction	40 μm PS	Focusing	100–300	–	[63]
		5/10 μm PS	Focusing	100 total		[42]
		15 μm PS	Trapping	40	800	[157]
		Yeast cells		10		
		10 μm PS	Trapping/patterning	125	~1,000	[158]
		Chinese hamster ovary cells	Electroporation Electrolysis	~400	~1,000	[159]
		Leukemia/red blood cells	Trapping/lysis	30	170	[161]
		5.7/15.7 μm PS	Separation	150	–	[162]
		Breast cancer cells	Separation	~100	–	[163]
		4T1 breast cancer cells/bone marrow cells	Separation and detection	~100	–	[164]
		0.5/2 μm PS	Separation	1,900	–	[166]
		Live/dead *E. coli* cells	Separation	~300	–	[167]
	1D widthwise post array	0.2 μm PS	Streaming	800	–	[173]
			Trapping	1,000		
		DNA	Trapping	N/A	1,000	[174]
		Live/dead *E. coli* cells	Trapping/separation	600	–	[175]
		Yeast cells	Trapping	~600	–	[184]
		200 nm PS	Trapping	~600	–	[185]
		DNA	Trapping/separation	26	660	[190]
		0.9/4.4 μm PS	Separation	−250−250	275, 450	[191]
		Protein	Trapping	120	–	[192]
	1D depthwise constriction	0.2 μm PS/*B. subtilis* cells	Separation	300	–	[195]

(*Continued*)

Table 2. Continued

Microchannel	Structure	Particles	Manipulation	Electric field (V/cm)		Refs.
				DC	AC	
		2/3 μm PS	Separation	50	750	[40]
		DNA	Separation	N/A	1.24 MV/m	[196]
		20/100 nm PS	Mixing/demixing	~10	625	[198]
	2D width/depth-wise constriction	10 μm PS/bacteria	Trapping	~50	–	[201]
		Staphylococcus *aureus*	Trapping	N/A	N/A	[203]
		Protein	Trapping	1.5	214	[205]
		Protein	Trapping	1.5	140	[206]
		DNA	Trapping	10	–	[207]
	Tunable droplet(s)	1/5.7/15.7 μm PS	Separation	80–240	–	[208]
		10 μm PS	Focusing/trapping	~200	–	[209]
Curved microchannels	Single bend	DNA	Deflection	~5	~5	[214]
		10 μm PS	Deflection	~100	–	[215]
	Serpentine	5/10 μm PS	Focusing	100/200	–	[218]
		Yeast/*E. coli* cells	Focusing/filtration	100 total	[219]	
		1/3 μm PS	Separation	55	825	[220]
		2.2/5 μm PS	Focusing/separation	~16	~176	[221]
		3 μm PS/yeast	Separation	100	–	[222]
	Spiral	10 μm PS	Focusing	100–200	–	[224]
		10 μm PS	Focusing	100–400	–	[225]
		5/10/15 μm PS	Separation	~350	–	[226]
		5/10/15 μm PS	Separation	~100	–	[227]
		5/10/10 μm PS	Separation by size/charge	~160	–	[228]
		5/3.5–6 μm PS	Separation by shape	~250	–	[229]
	Complex geometries	0.93 μm PS	Trapping	Up to 1 MV/m	–	[230]
		10/15 μm PS	Separation	130	–	[231]

microchannel [241] and the wall-directed particle migration in the DC electroosmotic flow of shear thinning fluids through straight rectangular microchannels [243]. Future work in this direction may cover the study of how the fluid rheological properties affect the electrokinetic motion of particles in varying microchannels, and as well the development of numerical models for understanding such motions with efficient algorithms and appropriate constitutive equations.

(2) Joule heating [199, 200] and induced charge [75, 244] effects have been usually deemed detrimental to precise electrokinetic transport and placement of particles in microchannels because of the induced electrothermal [96–99] and electroosmotic [119–125, 245] flows in high- and low-conductivity fluids, respectively. However, recent studies from the author's group [246, 247] have demonstrated the feasibility of using each of these nonlinear electrokinetic flow circulations to enrich submicron particles, which may potentially be applied to the continuous concentration of nanoparticles. Future work in this direction may cover the development of a general numerical model for an accurate and efficient simulation of both the fluid flows and the resulting particle trapping in a fluid with an arbitrary electric conductivity. For example, the author's group has recently developed a depth-averaged numerical model to understand and predict the Joule heating-induced electrothermal fluid flow [98] and induced charge electroosmotic fluid flow [245], respectively. This model can substantially reduce the computational cost for understanding the nonlinear electrokinetic phenomena and predicting the particle manipulation performance in microfluidic applications with shallow-channel geometries. Once verified and calibrated by experiments, the general numerical model can be used to optimize microchannel geometries for effective electrokinetic concentration of nanoparticles.

(3) A number of recent studies have reported interesting experimental observations of particle motions in combined DC electric field and pressure-driven flows of Newtonian fluids through straight microchannels. For example, Kim and Yoo demonstrated a 3D focusing along the axis of both a cylindrical [248] and a rectangular [249] microchannel for particles lagging behind the fluid flow because of negative electrophoresis. Such an electrophoretic slip-induced particle migration was later utilized by Yuan et al. [250] to switch the inertial particle focusing positions in a patterned straight rectangular microchannel via changing the DC electric field polarity. In a very recent experimental paper, Li and Xuan [251] reported exactly opposite particle migrations in an electro-hydrodynamic flow of viscoelastic fluid. They attributed the phenomena to the shear-induced extra lift that arises from the nonlinear coupling between particle electrophoresis and the local fluid flow [252, 253]. Interestingly, cross-stream migrations were also reported for DNA molecules in capillary electrophoresis with an applied Poiseuille flow though the moving direction seems also opposite to those of particles [254–258]. In addition, Yoda's group [259, 260] observed near-wall self-assembly of submicron polystyrene particles into streamwise bands in a counter-current Poiseuille and electroosmotic flow. Future work in this direction may cover the theoretical analysis of the inertial and/or elastic migration of electrophoretic particles in the Poiseuille-electroosmotic flow of Newtonian and non-Newtonian fluids, respectively. Further experimental studies on the comprehensive parametric effects (e.g., fluid rheological properties and particle properties) in such cross-stream particle migrations are also in need.

This work was supported in part by NSF under Grants CBET-0853873 and CBET-1704379, and as well by Clemson University through the Honors and Creative Inquiry programs. The author would like to thank the contributions from his current and previous PhD and master students: Mr. Christopher Church, Dr. Junjie Zhu, Mr. Sriram Sridharan, Mr. Litao Liang, Mr. John DuBose, Dr. Saurin Patel, Dr. Akshay Kale, Mr. Rama Prabhakaran, Dr. Xinyu Lu, Mr. Di Li, Mr. Zhijian Liu, and Mr. Amirreza Malekanfard. He also would like to thank the contributions from his undergraduate advisees, particularly Mr. Cameron Canter, Mr. Daniel Showers, Mr. Herbert Harrison, and Mr. Cory Thomas.

The author has declared no conflict of interest.

7 References

[1] Duffy, D. C., McDonald, J. C., Schueller, O. J. A., Whitesides, G. M., *Anal. Chem.* 1998, *70*, 4974–4984.

[2] Xuan, X., Zhu, J., Church, C., *Microfluid. Nanofluid.* 2010, *9*, 1–16.

[3] Huang, L., Bian, S., Cheng, Y., Shi, G., Liu, P., Ye, X., Wang, W., *Biomicrofluidics* 2017, *11*, 011501.

[4] Nilsson, J., Evander, M., Hammarstrom, B., Laurell, T., *Anal. Chimica Acta* 2009, *649*, 141–157.

[5] Sajeesh, P., Sen, A. K., *Microfluid. Nanofluid.* 2014, *17*, 1–52.

[6] Novo, P., Dell'Aica, M., Janasek, D., Zahedi, R. P., *Analyst* 2016, *141*, 1888–1905.

[7] Sibbitts, J., Sellens, K. A., Jia, S., Klasner, S. A., Culbertson, C. T., *Anal. Chem.* 2018, *90*, 65–85.

[8] Tasoglu, S., Gurkan, U. A., Wang, S. Q., Demirci, U., *Chem. Soc. Rev.* 2013, *42*, 5788–5808.

[9] Murphy, T. W., Zhang, Q., Naler, L. B., Ma, S., Lu, C., *Analyst* 2018, *143*, 60–80.

[10] Luo, T., Fan, L., Zeng, Y., Liu, Y., Chen, S., *Lab Chip* 2018, *18*, 1521–1532.

[11] Al-Faqheri, W., Thio, T. W. G., Qasaimeh, M. A., Dietzel, A., Madou, M., Al-Halhouli, A., *Microfluid. Nanofluid.* 2017, *21*, 102.

[12] Connacher, W., Zhang, N., Huang, A., Mei, J., Zhang, S., Gopesh, T., Friend, J., *Lab Chip* 2018, *18*, 1952–1996.

[13] Jubery, T. Z., Srivastava, S. K., Dutta, P., *Electrophoresis* 2014, *35*, 691–713.

[14] Munaz, A., Shiddiky, M. J. A., Nguyen, N. T., *Biomicrofluidics* 2018, *12*, 031501.

[15] Yang, H., Gijs, M. A. M., *Chem. Soc. Rev.* 2018, *47*, 1391–1458.

[16] Zhang, J., Yan, S., Yuan, D., Alici, G., Nguyen, N. T., Warkiani, M. E., Li, W., *Lab Chip* 2016, *16*, 10–34.

[17] Bousse, L., Cohen, C., Nikiforov, T., Chow, A., Kopf-Sill, A. R., Dubrow, R., Parce, J. W., *Annu. Rev. Biophys. Biomolecul. Struct.* 2000, *29*, 155–181.

[18] Wong, P. K., Chen, C., Wang, T., Ho, C., *Anal. Chem.* 2004, *76*, 6908–6914.

[19] Velev, O. D., Bhatt, K. H., *Soft Matt*. 2006, *2*, 738–750.

[20] Wong, P. K., Wang, T., Deval, J. H., Ho, C. M., *IEEE/ASME Trans. Mechatron.* 2004, *9*, 366–376.

[21] Salari, A., Thompson, M., *Sens. Actuat. B* 2018, *255*, 3601–3615.

[22] Chakraborty, S., *Electrophoresis* 2019, *40*, 180–189.

[23] Anderson, J. L., *Annu. Rev. Fluid. Mech.* 1989, *21*, 61–99.

[24] Di Carlo, D., *Lab Chip* 2009, *9*, 3038–3046.

[25] Li, D., *Electrokinetics in Microfluidics*. Elsevier Academic Press, Burlington 2004.

[26] Voldman, J., *Annu. Rev. Biomed. Eng.* 2006, *8*, 425–454.

[27] Chang, H. C., Yeo, L. Y., *Electrokinetically Driven Microfluidics and Nanofluidics*. Cambridge University Press, New York 2010.

[28] Pohl, H. A., *Dielectrophoresis*, Cambridge University Press, Cambridge 1978.

[29] Morgan, H., Green, N. G., *AC Electrokinetics: Colloids and Nanoparticles*. Research Studies Press, Philadelphia 2002.

[30] Pethig, R., *Biomicrofluidics* 2010, *4*, 022811.

[31] Kim, d., Sonker, M., Ros, A., *Anal. Chem.* 2019, *91*, 277–295.

[32] Kemp, G., *Biotechnol. Appl. Biochem.* 1998, *27*, 9–17.

[33] Masliyah, J. H., Bhattacharjee, S., *Electrokinetic and Colloid Transport Phenomena*. John Wiley & Sons, Hoboken 2006.

[34] Ramos, A., *Electrokinetics and Electrohydrodynamics in Microsystems*. Springer, Berlin 2011.

[35] Kang, Y, Li, D., *Microfluid. Nanofluid.* 2009, *6*, 431–460.

[36] Qian, S., Ai, Y., *Electrokinetic Particle Transport in Micro/Nanofluidics: Direct Numerical Simulation Analysis*. CRC Press, Boca Raton 2012.

[37] Srivastava, S. K., Gencoglu, A., Minerick, A. R., *Anal. Bioanal. Chem.* 2010, *399*, 301–321.

[38] Lapizco-Encinas, B. H., *Electrophoresis* 2019, *40*, 358–375.

[39] Prinz, C., Tegenfeldt, J. O., Austin, R. H., Cox, E. C., Sturm, J. C., *Lab Chip* 2002, *2*, 207–212.

[40] Hawkins, B. G., Smith, A. E., Syed, Y. A., Kirby, B. J., *Anal. Chem.* 2007, *79*, 7291–7300.

[41] Lewpiriyawong, N., Yang, C., Lam, Y. C., *Biomicrofluidics* 2008, *2*, 034105.

[42] Zhu, J., Xuan, X., *Electrophoresis* 2009, *30*, 2668–2675.

[43] Lyklemma, J., *Fundamentals of Interface and Colloid Science*. Academic Press, Cambridge 1991.

[44] Probstein, R. F., *Physicochemical Hydrodynamics*. John Willey and Sons, Hoboken 1994.

[45] Keh, H. J., Anderson, J. L., *J. Fluid. Mech.* 1985, *153*, 417–439.

[46] Hunter, R. J., *Zeta Potential in Colloid Science*. Academic Press, New York 1981.

[47] Happel, J., Brenner, H., *Low Reynolds Number Hydrodynamics*. Noordhoff International Publishing, Leyden 1973.

[48] Jones, T. B., *Electromechanics of Particles*. Cambridge University Press, New York City 1995.

[49] Yariv, E., *Phys. Fluid*. 2006, *18*, 031702.

[50] Keh, H. J., Lien, L. C., *J. Fluid Mech.* 1991, *224*, 305–333.

[51] Ennis, J., Anderson, J. L., *J. Colloid. Interf. Sci.* 1997, *185*, 497–514.

[52] Shugai, A., Carnie, S. L., *J. Colloid. Interf. Sci.* 1999, *213* 298–315.

[53] Tang, Y. P., Chih, M. H., Lee, E., Hsu, J. P., *J. Colloid Interf. Sci.* 2001, *242*, 121–126.

[54] Ye, C., Sinton, D., Erickson, D., Li, D., *Langmuir* 2002, *18*, 9095–9101.

[55] Yariv, E., Brenner, H., *SIAM J. Appl. Math.* 2003, *64*, 423–441.

[56] Hsu, J. P., Ku, M. H., Kao, C. Y., *J. Colloid Interf. Sci.* 2004, *276*, 248–254.

[57] Liu, H., Bau, H., Hu, H., *Langmuir* 2004, *20*, 2628–2639.

[58] Hsu, J. P., Kuo, C. C., *J. Phys. Chem. B* 2006, *110*, 17607–17615.

[59] Liu, H., Qian, S., Bau, H., *Biophys. J.* 2007, *92*, 1164–1177.

[60] Hsu, J. P., Chen, Z. S., *Langmuir* 2007, *23*, 6198–6204.

[61] Li, D., Daghighi, Y., *J. Colloid Interf. Sci.* 2010, *342*, 638–642.

[62] Ennis, J., Zhang, H., Stevens, G., Perera, J., Scales, P., Carnie, S., *J. Membr. Sci.* 1996, *119*, 47–58.

[63] Xuan, X., Raghibizadeh, S., Li, D., *J. Colloid Interf. Sci.* 2006, *296*, 743–748.

[64] Keh, H. J., Chen, S. B., *J. Fluid. Mech.* 198, 194, 377–390.

[65] Keh, H. J., Chiou, J. Y., *AICHE J.* 1996, *42*, 1397–1406.

[66] Yariv, E., Brenner, H., *Phys. Fluid.* 2002, *14*, 3354–3357.

[67] Yariv, E., Brenner, H., *J. Fluid Mech.* 2003, *484*, 85–111.

[68] Ye, C., Xuan, X., Li, D., *Microfluid. Nanofluid.* 2005, *1*, 234–241.

[69] Xuan, X., Ye, C., Li, D., *J. Colloid. Interf. Sci.* 2005, *289*, 286–290.

[70] Liang, Q., Zhao, C., Yang, C., *Electrophoresis* 2015, *36*, 731–736.

[71] Whitesides, G. M., Stroock, A. D., *Phys. Today* 2001, *54*, 42–48.

[72] Ghosal, S., *Annu. Rev. Fluid Mech.* 2006, *38*, 309–338.

[73] Henry, D. C., *Proc. Roy. Soc. London. Ser. A* 1931, *133*, 106–129.

[74] Bazant, M. Z., in: Li, D. (Ed.), *Encyclopedia of Microfluidics and Nanofluidics*, Part 14, Springer, Berlin, Heidelberg, New York 2008, pp. 1461–1470.

[75] Wang, Q., Dingari, N. N., Buie, C. R., *Electrophoresis* 2017, *38*, 2576–2586.

[76] Hughes, M. P., *Biomicrofluid*ics 2016, *10*, 032801.

[77] Pethig, R., *Adv. Drug Deliv. Rev.* 2013, *65*, 1589–1599.

[78] Nakano, A., Ros, A., *Electrophoresis* 2013, *34*, 1085–1096.

[79] Gascoyne, P. R. C., Shim, S., *Cancers* 2014, *6*, 545–579.

[80] Adekanmbi, E. O., Srivastava, S. K., *Lab Chip* 2016, *16*, 2148.

[81] Modarres, P., Tabrizian, M., *Sens. Actuat. B* 2017, *252*, 391–408.

[82] Gascoyne, P. R. C., Vykoukal, J., *Electrophoresis* 2002, *23*, 1973–1983.

[83] Hughes, M. P., *Electrophoresis* 2002, *23*, 2569–2582.

[84] Gascoyne, P. R. C., Vykoukal, J., *Proc. IEEE Inst. Electr. Electron. Eng.* 2004, *92*, 22–42.

[85] Jesu´s-Pe´rez, N. M., Lapizco-Encinas, B. H., *Electrophoresis* 2011, *32*, 2331–2357.

[86] Chou, C. F., Zenhausern, F., *IEEE Eng. Med. Biology Mag.* 2003, *22*, 62–67.

[87] Cummings, E. B., *IEEE Eng. Med. Biology Mag.* 2003, *22*, 75–84.

[88] Regtmeier, J., Eichhorn, R., Viefhues, M., Bogunovic, L., Anselmetti, D., *Electrophoresis* 2011, *32*, 2253–2273.

[89] Li, M., Li, W. H., Zhang, J., Alici, G., Wen, W., *J. Phys. D: Appl. Phys.* 2014, *47*, 063001.

[90] Lapizco-Encinas, B. H., Rito-Palmomares, M. *Electrophoresis* 2007, *28*, 4521–4538.

[91] Gagnon, Z. R., *Electrophoresis* 2011, *32*, 2466–2487.

[92] Cetin, B., Li, D., *Electrophoresis* 2011, *32*, 2410–2427.

[93] Dash, S., Mohanty, S., *Electrophoresis* 2014, *35*, 2656–2672.

[94] Ramos, A., Morgan, H., Green, N. G., Castellanos, A. C., *J. Phys. D* 1998, *31*, 2338–2353.

[95] Casterllanos, A., Ramos, A., Gonzalez, A., Green, N. G., Morgan, H., *J. Phys. D* 2003, *36*, 2584–2597.

[96] Hawkins, B. J., Kirby, B. J., *Electrophoresis* 2010, *31*, 3622–3633.

[97] Sridharan, S., Zhu, J., Hu, G., Xuan, X., *Electrophoresis* 2011, *32*, 2274–2281.

[98] Prabhakaran, R. A., Zhou, Y., Patel, S., Kale, A., Song, Y., Hu, G., Xuan, X., *Electrophoresis* 2017, *38*, 572–579.

[99] Gonzalez A, Ramos A, Morgan H, Green, N. G., Castellanos, A. C., *J. Fluid Mech.* 2006, *564*, 415–433.

[100] Chaurey, V., Polanco, C., Chou, C. F., Swami, N. S., *Biomicrofluid*ics 2012, *6*, 012806.

[101] Zhu, J., Sridharan, S., Hu, G., Xuan, X., *J. Micromechan. Microeng.* 2012, *22*, 075011.

[102] Kale, A., Patel, S., Hu, G., Xuan, X., *Electrophoresis* 2013, *34*, 674–683.

[103] Kale, A., Patel, S., Qian, S., Hu, G., Xuan, X., *Electrophoresis* 2014, *35*, 721–727.

[104] Gallo-Villanueva, R., Sano, M., Lapizco-Encinas, B., Davalos, R., *Electrophoresis* 2014, *35*, 352–361.

[105] Bazant, M. Z., Squires, T. M., *Phys. Rev. Lett.* 2004, *92*, 066101.

[106] Squires, T. M., Bazant, M. Z., *J. Fluid. Mech.* 2004, *509*, 217–252.

[107] Ramos, A., Morgan, H., Green, N. G., Castellanos, A., *J. Colloid Interface Sci.* 1999, *217*, 420–422.

[108] Green, N. G., Ramos, A., González, A., Morgan, H., Castellanos, A., *Phys. Rev. E* 2000, *61*, 4011.

[109] Levitan, J. A., Devasenathipathy, S., Studer, V., Ben, Y., Thorsen, T., Squires, T. M., Bazant, M. Z., *Colloid. Surf. A* 2005, *267*, 122–132.

[110] Ajdari, A., *Phys. Rev. E* 2000, *61*, R45–R48.

[111] Wong, P. K., Chan, C. Y., Wang, T. H., Ho, C. M., *Anal. Chem.* 2004, *76*, 6908–6914.

[112] Squires, T. M., Bazant, M. Z., *J. Fluid Mech.* 2006, *560*, 65–101.

[113] Bazant, M. Z., Squires, T. M., *Current Opin. Colloid Interf. Sci.* 2010, *15*, 203–213.

[114] Huang, C. C.; Bazant, M. Z.; Thorsen, T., *Lab Chip* 2010, *10*, 80–85.

[115] Yalcin, S. E., Sharma, A., Qian, S., Joo, S. W., Baysal, O., *Electrophoresis* 2010, *31*, 3711–3718.

[116] Ren, Y., Liu, W., Jia, Y., Tao, Y., Shao, J., Ding, Y., Jiang, H., *Lab Chip* 2015, *15*, 2181–2191.

[117] Tao, Y., Ren, Y., Liu, W., Wu, Y., Jia, Y., Lang, Q., Jiang, H., *Electrophoresis* 2016, *37*, 1326–1336.

[118] Nadal, F., Argoul, F., Kestener, P., Pouligny, B., Ybert, C., Ajdari, A., *Eur. Phys. J. E* 2002, *9*, 387–399.

[119] Chen, J. K., Yang, R. J., *Microfluid. Nanofluid.* 2008, *5*, 719–725.

[120] Eckstein, Y., Yossifon, G., Seifert, A., Miloh, T., *J. Colloid Interf. Sci.* 2009, *338*, 243–249.

[121] Sherwood, J. D., Mao, M., Ghosal, S., *Phys. Fluid.* 2014, *26*, 112004.

[122] Takhistov, P., Duginova, K., Chang, H.-C., *J. Colloid Interf. Sci.* 2003, *263*, 133–143.

[123] Yossifon, G., Frankel, I., Miloh, T., *Phys. Fluid.* 2006, *18*, 117108.

[124] Thamida, S., Chang, H.-C., *Phys. Fluid.* 2002, *14*, 4315–4328.

[125] Zehavi, M., Yossifon, G., *Phys. Fluid.* 2014, *26*, 082002.

[126] Santiago, J. G., *Anal. Chem.* 2001, *73*, 2353–2365.

[127] Young, E., Li, D., *Langmuir* 2005, *21*, 12037–12046.

[128] Kang, K., Xuan, X., Kang, Y., Li, D., *J. Appl. Phys.* 2006, *99*, 064702.

[129] Zhao, H., Bau, H., *Langmuir* 2007, *23*, 4053−4063.

[130] Lo, Y. J., Lei, U., *Appl. Phys. Lett.* 2009, *95*, 253701.

[131] Lo, Y. J., Lei, U., *Appl. Phys. Lett.* 2010, *97*, 093702.

[132] Kang, S., *J. Electrostat.* 2015, *76*, 159–170.

[133] Yoda, M., Kazoe, Y., *Phys. Fluid.* 2011, *23*, 111301.

[134] Kazoe, Y., Yoda, M., *Langmuir* 2011, *27*, 11481–11488.

[135] Yariv, E., *Soft Matt.* 2016, *12*, 6277–6284.

[136] Delgado, A. V., González-Caballero, F., Hunter, R. J., Koopal, L. K., Lyklema, J., *J. Colloid Interf. Sci.* 2007, *309*, 194–224.

[137] Saville, D. A., *Annu. Rev. Fluid Mech.* 1977, *9*, 321–337.

[138] Ai, Y., Beskok, A., Gauthier, D. T., Joo, S. W., Qian, S., *Biomicrofluidics* 2009, *3*, 044110

[139] Liang, L., Ai, Y., Zhu, J., Qian, S., Xuan, X., *J. Colloid Interf. Sci.* 2010, *347*, 142–146.

[140] Liang, L., Qian, S., Xuan, X., *J. Colloid Interf. Sci.* 2010, *350*, 377–379.

[141] Liu, Z., Li, D., Song, Y., Pan, X., Li, D., Xuan, X., *Phys. Fluid.* 2017, *29*, 102001.

[142] Kirby, B. J., Hasselbrink, E. F., Jr., *Electrophoresis* 2004, *25*, 203–213.

[143] Liu, Z., Li, D., Saffarian, M., Tzeng, T.-R, Song, Y., Pan, X., Xuan, X., *Electrophoresis* 2019, *40*, 955–960.

[144] Lu, X., Hsu, J. P., Xuan, X., *Langmuir* 2015, *31*, 620–627.

[145] Li, D., Lu, X., Song, Y., Wang, J., Li, D., Xuan, X., *Biomicrofluidics* 2016, *10*, 054104.

[146] Thomas, C., Lu, X., Todd, A., Raval, Y., Tzeng, T., Song, Y., Wang, J., Li, D., Xuan, X., *Electrophoresis* 2017, *38*, 320–326.

[147] Li, M., Li, D., *J. Chromatography A* 2017, *1501*, 151–160.

[148] Xuan, X., Reservoir-Based Dielectrophoresis. in: Li, D. (Ed.), *Encyclopedia of Microfluidics and Nanofluidics*. Springer, New York, NY. https://doi.org/10.1007/978-1-4614-5491-5_1743.

[149] Zhu, J., Hu, G., Xuan, X., *Electrophoresis* 2012, *33*, 916–922.

[150] Zhu, L., Patel, S., Johnson, M., Kale, A., Raval, Y., Tzeng, T. R., Xuan, X., *Micromachines* 2016, *7*, 156.

[151] Kale, A., Patel, S., Xuan, X., *Micromachines* 2018, *9*, 123.

[152] Patel, S., Qian, S., Xuan, X., *Electrophoresis* 2013, *34*, 961–968.

[153] Patel, S., Showers, D., Vedantam, P., Tzeng, T., Qian, S., Xuan, X., *Biomicrofluidics* 2012, *6*, 034102.

[154] Pethig, R., Marks, G. H., *Trend. Biotechnol.* 1997, *15*, 426–432.

[155] Xuan, X., Xu, B., Li, D., *Anal. Chem.* 2005, *77*, 4323–4328.

[156] Ai, Y., Joo, S., Jiang, Y., Xuan, X., Qian, S., *Electrophoresis* 2009, *30*, 2499–2506.

[157] Lewpiriyawong, N., Yang, C., Lam, Y.C., *Microfluid. Nanofluid.* 2012, *12*, 723–733.

[158] Kale, A., Lu, X., Patel, S., Xuan, X., *J. Micromech. Microeng.* 2014, *24*, 075007.

[159] Wang, H., Lu, L., *Anal. Chem.* 2006, *78*, 5158–5164.

[160] Wang, H., Bhunia, A. K., Lu, C., *Biosens. Bioelectron.* 2006, *22*, 582–588.

[161] Church, C., Zhu, J., Huang, G., Tzeng, T., Xuan, X., *Biomicrofluidics* 2010, *4*, 044101.

[162] Kang, K., Kang, Y., Xuan, X., Li, D., *Electrophoresis* 2006, *27*, 694–702.

[163] Kang, Y. J., Li, D. Q., Kalams, S. A., Eid, J. E., *Biomed. Microdev.* 2008, *10*, 243–249.

[164] Sun, J., Gao, Y., Isaacs, R. J., Boelte, K. C., Lin, P. C., Boczko, E. M., Li, D., *Anal. Chem.* 2012, *84*, 2017–2024.

[165] Abdallah, B. G., Chao, T., Kupitz, C., Fromme, P., Ros, A., *ACS Nano* 2013, *7*, 9129–9137.

[166] Abdallah, B. G., Roy-Chowdhury, S., Coe, J., Fromme, P., Ros, A., *Anal. Chem.* 2015, *87*, 4159–4167.

[167] Pysher, M. D., Hayes, M. A., *Anal. Chem.* 2007, *79*, 4552–4557.

[168] Ding, J., Woolley, C., Hayes, M. A., *Anal. Bioanal. Chem.* 2017, *409*, 6405–6414.

[169] Staton, S. J., Chen, K. P., Taylor, T. J., Pacheco, J. R., Hayes, M. A., *Electrophoresis* 2010, *31*, 3634–3641.

[170] Mohammadi, M., Madadi, H., Casals-Terré, J., Sellarès, J., *Anal. Bioanal. Chem.* 2015, *407*, 4733–4744.

[171] Mohammadi, M., Madadi, H., Casals-Terré, J., Sellarès, J., *Biomicrofluidics* 2015, *9*, 054106.

[172] Cummings, E. B., Singh, A. K., *Proceedings SPIE 4177, Microfluidic Devices and Systems III*, Santa Clara, CA 2000. https://doi.org/10.1117/12.395653

[173] Cummings, E. B., Singh, A. K., *Anal. Chem.* 2003, *75*, 4724–4731.

[174] Chou, C. F., Tegenfeldt, J. O., Bakajin, O., Chan, S. S., Cox, E. C., Darnton, N., Duke, T., Austin, R. H, *Biophys. J.* 2002, *83*, 2170–2179.

[175] Lapizco-Encinas, B. H., Simmons, B. A., Cummings, E. B., Fintschenko, Y., *Anal. Chem.* 2004, *76*, 1571–1579.

[176] Lapizco-Encinas, B. H., Simmons, B. A., Cummings, E. B., Fintschenko, Y., *Electrophoresis* 2004, *25*, 1695–1704.

[177] Ozuna-Chacón, S., Lapizco-Encinas, B. H., Rito-Palomares, M., Martínez-Chapa, S. O., Reyes-Betanzo, C., *Electrophoresis* 2008, *29*, 3115–3122.

[178] Gallo-Villanueva, R. C., Pe´rez-Gonza´lez, V. H., Davalos, R. V., Lapizco-Encinas, B. H., *Electrophoresis* 2011, *32*, 2456–2465.

[179] LaLonde, A., Gencoglu, A., Romero-Creel, M. F., Koppula, K. S., Lapizco-Encinas, B. H., *J. Chromatogra. A* 2014, *1344*, 99–108.

[180] Saucedo-Espinosa, M. A., Lapizco-Encinas, B. H., *Electrophoresis* 2015, *36*, 1086–1097.

[181] Saucedo-Espinosa, M. A., LaLonde, A., Gencoglu, A., Romero-Creel, M. F., Dolas, J. R., Lapizco-Encinas, B. H., *Electrophoresis* 2016, *37*, 282–290.

[182] Lapizco-Encinas, B. H., Ozuna-Chaco´n, S., Rito-Palomares, M., *J. Chromatogra. A* 2008, *1206*, 45–51.

[183] Rosales-Cruzaley, E., Cota-Elizondo, P. A., Sánchez, D., Lapizco-Encinas, B. H., *Bioprocess Biosys. Eng.* 2013, *36*, 1353–1362.

[184] Saucedo-Espinosa, M. A., Lapizco-Encinas, B. H., *Anal. Chem.* 2017, *89*, 8459−8467.

[185] Perez-Gonzalez, V. H., Gallo-Villanueva, R. C., Cardenas-Benitez, B., Martinez-Chapa, S. O., Lapizco-Encinas, B. H., *Anal. Chem.* 2018, *90*, 4310–4315.

[186] Nakano, A., Chao, T., Camacho-Alanis, F., Ros, A., *Electrophoresis* 2011, *32*, 2314–2322.

[187] Nakano, A., Camacho-Alanis, F., Chao, T., Ros, A., *Biomicrofluidics* 2012, *6*, 034108.

[188] Gan, L., Chao, T., Camacho-Alanis, F., Ros, A., *Anal. Chem.* 2013, *85*, 11427−11434.

[189] Rabbani, M. T., Schmidt, C. F., Ros, A., *Anal. Chem.* 2017, *89*, 13235–13244.

[190] Regtmeier, J., Duong, T. T., Eichhorn, R., Anselmetti, D., Ros, A., *Anal. Chem.* 2007, *79*, 3925–3932.

[191] Luo, J., Muratore, K. A., Arriaga, E. A., Ros, A., *Anal. Chem.* 2016, *88*, 5920–5927.

[192] Nakano, A., Camacho-Alanis, F., Ros, A., *Analyst* 2015, *140*, 860–868.

[193] Davalos, R. V., McGraw, G. J., Wallow, T. I., Morales, A. M., Krafcik, K. L., Fintschenko, Y., Cummings, E. B., Simmons, B. A., *Anal. Bioanal. Chem.* 2008, *390*, 847–855.

[194] Sabounchi, P., Morales, A. M., Ponce, P., Lee, L. P., Simmons, B. A., Davalos, R. V., *Biomed. Microdev.* 2008, *10*, 661–670.

[195] Barrett, L. M., Skulan, A. J., Singh, A. K., Cummings, E. B., Fiechtner, G. J., *Anal. Chem.* 2005, *77*, 6798–6804.

[196] Täuber, S., Kunze, L., Grauberger, O., Grundmann, A., Viefhues, M., *Analyst* 2017, *142*, 4670–4677.

[197] Viefhues, M., Wegener, S., Rischmüller, A., Schleef, M., Anselmetti, D., *Lab Chip* 2013, *13*, 3111–3118.

[198] Viefhues, M., Eichhorn, R., Fredrich, E., Regtmeier, J., Anselmetti, D., *Lab Chip* 2012, *12*, 485–494.

[199] Xuan, X., *Electrophoresis* 2008, *29*, 33–43.

[200] Cetin, B., Li, D. Q., *Electrophoresis* 2008, *29*, 994–1005.

[201] W. A. Braff, A. Pignier, C. R. Buie, *Lab Chip* 2012, *12*, 1327–1331.

[202] Braff, W. A., Willner, D., Hugenholtz, P., Rabaey, K., Buie, C. R., *PLoS ONE* 2013, *8*, e76751. https://doi.org/10.1371/journal.pone.0076751

[203] Nakidde, D., Zellner, P., Alemi, M. M., Shake, T., Hosseini, Y., Riquelme, M. V., Pruden, A., Agah, M., *Biomicrofluidics* 2015, *9*, 014125.

[204] Zellner, P., Shake, T., Hosseini, Y., Nakidde, D., Riquelme, M. V., Sahari, A., Pruden, A., Behkam, B., Agah, M., *Electrophoresis* 2015, *36*, 277–283.

[205] Liao, K. T., Chou, C. F., *J. Am. Chem. Soc.* 2012, *134*, 8742–8745.

[206] Liao, K. T., Tsegaye, M., Chaurey, V., Chou, C. F., Swami, N. S., *Electrophoresis* 2012, *33*, 1958–1966.

[207] Li, S., Ye, Z., Hui, Y. S., Gao, Y., Jiang, Y., Wen, W., *Biomicrofluidics* 2015, *9*, 054115.

[208] Barbulovic-Nad, I., Xuan, X., Lee, J. S., Li, D., *Lab Chip* 2006, *6*, 274–279.

[209] Thwar, P. K., Linderman, J. J., Burns, M. A., *Electrophoresis* 2007, *28*, 4572–4581.

[210] Kirby, B. J., *Micro and Nanoscale Fluid Mechanics: Transport in Microfluidic Devices*. Cambridge University Press, New York 2010.

[211] Xuan, X., Curvature-Induced Dielectrophoresis. in: Li, D. (Ed.), *Encyclopedia of Microfluidics and Nanofluidics*. Springer, Boston, MA. https://doi.org/10.1007/978-3-642-27758-0_1742-1

[212] Ye, C., Li, D., *J. Colloid Interf. Sci.* 2004, *272*, 480–488.

[213] Davison, S. M., Sharp, K. V., *Microfluid. Nanofluid.* 2008, *4*, 409–418.

[214] Parikesit, G. O., Markesteijn, A. P., Piciu, O. M., Bossche, A., Westerweel, J., Young, I. T., Garini, Y., *Biomicrofluidics* 2008, *2*, 24103.

[215] Ai, Y., Park, S., Zhu, J., Xuan, X., Beskok, A., Qian, S., *Langmuir* 2010, *26*, 2937–2944.

[216] House, D. L., Luo, H., *Electrophoresis* 2011, *32*, 3277–3285.

[217] Cetin, B., Oner, S. D., Baranoglu, B., *Electrophoresis* 2017, *38*, 1407–1418.

[218] Zhu, J., Tzeng, T. J., Hu, G., Xuan, X., *Microfluid. Nanofluid.* 2009, *7*, 751–756.

[219] Church, C., Zhu, J., Wang, G., Tzeng, T. J., Xuan, X., *Biomicrofluidics* 2009, *3*, 044109.

[220] Church, C.; Zhu, J., Xuan, X., *Electrophoresis* 2011, *32*, 527–531.

[221] Church, C., Zhu, J., Nieto, J., Keten, G., Ibarra, E., Xuan, X., *J. Micromech. Microeng.* 2010, *20*, 065011.

[222] Zhu, J., Canter, R., Keten, G., Vedantam, P., Tzeng, T. R., Xuan, X., *Microfluid. Nanofluid.* 2011, *11*, 743–752.

[223] Zhang, L., Tatar, F., Turmezei, P., Bastemeijer, J., Mollinger, J. R., Piciu, O., Bossche, A., *J. Phys.: Conference Series* 2006, *34*, 527–532.

[224] Zhu, J., Tzeng, J. T., Xuan, X., *Proceeding of ASME 2009 International Mechanical Engineering Congress and Exposition, IMECE2009-11876*, Lake Buena Vista, FL 2009.

[225] Zhu, J., Xuan, X., *J. Colloid Interf. Sci.* 2009, *340*, 285–290.

[226] DuBose, J., Zhu, J., Patel, S., Lu, X., Tupper, N., Stonaker, J. M., Xuan, X., *J. Micromech. Microeng.*2014, *24*, 115018.

[227] Zhu, J., Tzeng, T. J., Xuan, X., *Electrophoresis* 2010, *31*, 1382–1388.

[228] Zhu, J., Xuan, X., *Biomicrofluid*ics 2011, *5*, 024111.

[229] DuBose, J., Lu, X., Patel, S., Qian, S., Joo, S., Xuan, X., *Biomicrofluid*ics 2014, *8*, 014101.

[230] Chen, D., Du, H., *Microfluid. Nanofluid.* 2010, *9*, 281–291.

[231] Li, M., Li, S., Li, W., Wen, W., Alici, G., *Electrophoresis* 2013, *34*, 952–960.

[232] Youssefi, M. R., Diez, F. J., *Electrophoresis* 2016, *37*, 692–698.

[233] Bazant, M. Z., Kilic, M. S., Storey, B. D., Ajdari, A., *Adv. Colloid Interf. Sci.* 2009, *152*, 48–88.

[234] Bird, R. B., Armstrong, R. C., Hassager, O., *Dynamics of Polymeric Liquids*. Vol. *1*, Wiley-Interscience, 1977.

[235] Gupta, S., Wang, W. S., Vanapalli, S. A., *Biomicrofluid*ics 2016, *10*, 043402.

[236] Zhao, C., Yang, C., *Adv. Colloid Interf. Sci.* 2013, *201*, 94–108.

[237] D'Avino, G., Greco, F., Maffettone, P. L., *Annu. Rev. Fluid Mech.* 2017, *49*, 341–360.

[238] Lu, X., Liu, C., Hu, G., Xuan, X., *J. Colloid Interf. Sci.* 2017, *500*, 182–201.

[239] Liu, C., Hu, G., *Micromachines* 2017, *8*, 73.

[240] Yuan, D., Zhao, Q., Yan, S., Tang, S. Y., Alici, G., Zhang, J., Li, W., Lab Chip 2018, *18*, 551–567.

[241] Lu, X., Patel, S., Zhang, M., Joo, S., Qian, S., Ogale, A., Xuan, X., *Biomicrofluid*ics 2014, *8*, 021802.

[242] Lu, X., DuBose, J., Qian, S., Joo, S., Xuan, X., *Biomicrofluid*ics 2015, *9*, 014108.

[243] Malekanfard, A., Ko, C. H., Li, D., Bulloch, L, Baldwin, A., Wang, Y. N., Fu, L. M., Xuan, X., *Phys. Fluid.* 2019, *31*, 022002.

[244] Zehavi, M., Boymelgreen, A., Yossifon, G., *Phys. Rev. Appl.* 2016, *5*, 044013.

[245] Prabhakaran, R. A., Zhou, Y., Zhao, C., Hu, G., Song, Y., Wang, J., Yang, C., Xuan, X., *Phys. Fluid.* 2017, *29*, 062001.

[246] Kale, A., Song, L., Lu, X., Yu, L., Hu, G., Xuan, X., *Electrophoresis* 2018, *39*, 887–896.

[247] Harrison, H., Lu, X., Patel, S., Thomas, C., Todd, A., Johnson, M., Raval, Y., Tzeng, T., Song, Y., Wang, J., Li, D., Xuan, X, *Analyst* 2015, *140*, 2869–2875.

[248] Kim, Y. M., Yoo, J. Y., *Lab Chip* 2009, *9*, 1043–1045.

[249] Kim, Y. M., Yoo, J. Y., *J. Micromech. Microeng.* 2015, *25*, 027002.

[250] Yuan, D., Pan, C., Zhang, J., Yan, S., Zhao, Q., Alici, G., Li, W., *Micromachines* 2016, *7*, 195.

[251] Li, D., Xuan, X., *Phys. Rev. Fluid.* 2018, *3*, 074202.

[252] Vishnampet, R., Saintillan, D., *Phys. Fluid.* 2012, *24*, 073302.

[253] Einarsson, J., Mehlig, B., *Phys. Rev. Fluids* 2017, *2*, 063301.

[254] Zheng, J., Yeung, E. S., *Anal. Chem.* 2002, *74*, 4536–4547.

[255] Zheng, J., Yeung, E. S., *Anal. Chem.* 2003, *75*, 3675–3680.

[256] Arca, M., Butler, J. E., Ladd, A. J. C., *Soft Matt.* 2015, *11*, 4375–4382.

[257] Arca, M., Ladd, A. J. C., Butler, J. E., *Soft Matt.* 2016, *12*, 6975–6984.

[258] Montes, R. J., Butler, J. E., Ladd, A. J. C., *Electrophoresis* 2019, *40*, 437–446.

[259] Cevheri, N., Yoda, M., *Lab Chip* 2014, *14*, 1391–1394.

[260] Yee, A., Yoda, M., *Microfluid. Nanofluid.* 2018, *22*, 113.

